Atypical functional connectome in congenitally blind humans

Cemal Koba[1]*, Joan Falcó-Roget[1], Olivier Collignon[2,3], Katarzyna Rączy[4,5], Marina Bedny[6], Mengyu Tian[7], Marcin Szwed[4]†, Anna-Lena Stroh[4]*†

Keywords: brain plasticity; development; gradients; vision; hierarchy

[1] Sano - Centre for Computational Medicine, Czarnowiejska 36, 30-054, Kraków, Poland

[2] Institute of Psychology (IPSY) & Institute of Neuroscience (IoNS), UCLouvain, Louvain-la-Neuve 1348, Belgium.

[3] The Sense Innovation and Research Center, Lausanne 1007 & Sion 1950, Switzerland

[4] Institute of Psychology, Jagiellonian University, Kraków, Poland

[5] Biological Psychology and Neuropsychology, University of Hamburg, 20146 Hamburg, Germany

[6] Department of Psychological and Brain Sciences, Johns Hopkins University, Baltimore, MD, USA

[7] Institute of Advanced Studies in Humanities and Social Sciences, Beijing Normal University, Zhuhai 519087, China
* corresponding authors

† shared senior authorship

Author contributions

Cemal Koba: Conceptualization, Methodology, Software, Formal analysis, Data curation, Writing - Original Draft, Writing - Review & Editing, Visualization, **Joan Falco Roget:** Methodology, Writing - Review & Editing, **Olivier Collignon:** Funding acquisition, Data acquisition, **Katarzyna Raczy:** Investigation, Data curation, Writing - Review & Editing, **Marina Bedny:** Funding acquisition, Data acquisition, Writing - Review & Editing, **Mengyu Tian:** data curation **Marcin Szwed:** Funding acquisition, Data acquisition, Writing - Review & Editing, Supervision **Anna-Lena Stroh:** Conceptualization, Methodology, Software, Formal analysis, Data curation, Writing - Original Draft, Writing - Review & Editing, Visualization, Supervision

Abstract

The cortex is organized along macroscale structural and functional gradients that extend from unimodal to transmodal association areas and from somatosensory to visual regions. It has not been tested whether this organization represents an intrinsic neuro-architecture immune to sensory experience or depends on sensory input. Here, we conducted connectome gradient analyses using resting-state functional Magnetic Resonance Imaging in congenitally blind individuals and sighted controls. In both groups, we observed a principal gradient (G1) extending from unimodal to transmodal, a second gradient (G2) spanning from somatosensory to visual, and a third gradient (G3) separating the frontoparietal network from the rest of the brain. Our findings indicate that the macroscale organization of the cortex develops largely independently of sensory experience. However, in blind individuals, the sensorimotor network was more distanced from the visual network (G2), while the visual network was more integrated with transmodal (G1) and frontoparietal (G3) networks. In blind individuals, the hierarchical organization within the early visual cortex was altered, the structure-function coupling in visual and temporal areas was reduced, and functional similarity between V1 center and periphery disappeared. These results suggest a critical role of sensory input in shaping the macroscale functional and structural organization of the brain.

1 - Introduction

The cortex is organized along macroscale functional and structural gradients that extend from unimodal (somatosensory/motor and visual) to transmodal association areas, and from somatosensory to visual areas[1,2]. This organization is hypothesized to be essential for the emergence of abstract, higher-order cognitive functions in transmodal, integrative cortices by isolating them from the processing of incoming environmental information[1,2]. However, whether this core organizing axis is an intrinsic neuro-architecture immune to experience or, instead, depends on sensory input during development has not been tested. The study of sensory deprived individuals can provide unique insights into this issue, as it can reveal how the lack of sensory input into one sensory network changes the functional architecture not only within this network but across the broader cortex. To address this question, we compared functional connectivity gradients and their relationship to structural measurements between blind and sighted individuals.

Numerous studies have shown that blindness results in significant differences in the functional and structural organization of the brain. For example, several studies have reported changes in resting state functional connectivity (rsFC), including a decrease of rsFC between visual and sensorimotor areas[3,4] and an increase between the visual cortex and the lateral prefrontal, parietal, and temporal cortices[3,5–9]. In addition to these functional changes, several structural changes have been observed in blind individuals, including increased cortical thickness[10–13] and a reduction of the surface area of V1[11,14]. Moreover, there is ample evidence to suggest that the visual cortex of blind individuals can adapt to process auditory and tactile input[15], demonstrating that the sensory modality of a region is not fixed and can be changed by experience. Crucially, in blind individuals, visual cortices, including V1, do not only respond to low-level tactile and auditory stimulation, but also seem to be involved in higher-level functions, such as language[3,16], numerical cognition[17], and executive functioning[5,18]. These latter findings could suggest that congenital blindness leads to alterations of the cortical hierarchy[19].

So far, neuroimaging studies in blind humans have not been able to successfully probe the hierarchical organization within the visual system and across the broader cortex. However, new developments in the analysis of resting-state functional magnetic resonance imaging (rs-fMRI) data now make it feasible to study functional hierarchies non-invasively. Connectome compression techniques have revealed three principal gradients of connectivity differentiation along the cortical surface[1]. The principal gradient extends from unimodal to transmodal areas and closely corresponds to classic models of the cortical hierarchy[2,20], thus making it ideally suited to investigate the effects of sensory experience on the development of the cortical hierarchy. The second gradient spans between the visual and sensorimotor systems[1], differentiating regions depending on their involvement in modality-specific processing. The third gradient extends between areas of the brain that are typically involved in attentional modulation (fronto-parietal attention and control networks) and those that are involved in content representation (default mode (DMN), sensorimotor (SMN) and visual networks (VN))[21,22]. Together, these three gradients describe a functional organization in which primary sensory and transmodal regions exhibit functional segregation, while the ventral attention network exhibits functional integration[23–25].

Gradients are valuable not only for studying the relationships between different cortical networks but also for mapping the functional organization within networks[26,27]. Previous studies have used this approach to study the hierarchical organization within multiple brain regions, such as the primary somatosensory cortex[28], the angular gyrus[29], and the insula[30,31]. These studies have revealed several gradients that have shown a strong correspondence with canonical functional networks and corresponding behavioral domains[29–32], geometric distance[32], cortical morphology[32] and microstructure[28], as well as gene expression[29]. Moreover, previous studies have used rsFC gradients for cortical area parcellations and it has been shown that they exhibit strong correspondence with task activation maps and with probabilistic V1 and V2[33,34]. Here, we used rsFC gradients to investigate the impact of visual deprivation on the functional hierarchical organization within the visual cortex, including early, ventral, dorsal, and lateral visual areas.

The structural organization of the human cortex seems to follow similar macroscale gradients as the functional organization. A tight coupling between structure and function has been observed within primary sensory and motor areas, whereas in transmodal association areas, structure and function seem to diverge[35–38]. Although numerous studies have investigated both structural and functional plasticity in blind individuals, the coupling between the two remains largely underexplored. Further examining these relationships could provide valuable insights into how cortical structure adapts to support the higher-level functions associated with the visual cortices of blind individuals.

In summary, we aimed to assess to what extent the core organizing axis of the human cortex depends on sensory input during development. First, we compared macroscale functional connectivity gradients between congenitally blind and sighted individuals. In addition, we investigated how the functional organization *within* the visual system depends on sensory input during development by comparing connectopic maps of the visual system between blind and sighted individuals. Finally, we examined how the structure of the (visual) cortex changes, in order to accommodate the new higher-level functions that have been associated with the visual cortices of blind individuals. To this end, we compared structure-function coupling between the functional connectivity gradients and a principal component derived from structural features including cortical thickness, curvature, sulcal depth, surface area, and volume.

2 - Methods

2.1 Datasets

2.1.1 Dataset 1

Complete details of the dataset and imaging parameters are given in Pelland et al. [39]. The entire dataset included 50 individuals who participated in a single five-minute functional MRI run (136 volumes). Participants were instructed to keep their eyes closed, relax, and not think about anything in particular. Functional time series were acquired using a 3-T TRIO TIM (Siemens) equipped with a 12-channel head

coil. Multislice T2*- weighted fMRI images were obtained with a gradient echo-planar sequence using axial slice orientation; repetition time (TR) 2200 ms; echo time (TE) 30 ms; functional anisotropy (FA) 90 degrees; 35 transverse slices; 3.2 mm slice thickness; 0.8 mm gap; field of view (FoV) 192 X 192 mm^2; matrix size 64 x 64 x 35; voxel size 3 x 3 x 3.2 mm^3 . A structural T1-weighted 3D magnetization prepared rapid gradient echo sequence (voxel size 1 x 1 x 1.2 mm^3; matrix size 240 x 256 ; TR 2300 ms; TE 2.91 ms; TI 900 ms; FoV 256; 160 slices) was also acquired for all participants. All of the procedures were approved by the Research Ethic and Scientific Boards of the Centre for Interdisciplinary Research in Rehabilitation of Greater Montreal and the Quebec Bio-Imaging Network. Experiments were undertaken with the understanding and written consent of each participant.

The dataset consisted of 50 participants, including both congenitally blind and late blind participants and the respective sighted matches. In this study, we focused on the group of congenitally blind individuals and their sighted controls. The final sample thus included 28 participants, including 14 congenitally blind individuals (9 males, 5 females, mean age 43.93 ± 11.19 years, 12 right-handed, 2 ambidextrous), and 14 sighted controls, who were matched for age and sex with the sample of congenitally blind individuals (sighted controls: mean age 40.92±13.64 years, 7 males, 7 females, 13 right-handed, 1 left-handed). The dataset was made available in the Brain Imaging Data Structure (BIDS[40]) format. Along with the folder and naming standardization, the first four volumes of functional runs were removed to avoid stabilization artifacts (leaving 132 volumes in total), and the resolution of the functional runs was interpolated to 3 x 3 x 4 mm^3. The data providers confirmed that no other preprocessing steps were applied during the standardization procedure.

2.1.2 Dataset 2

The dataset was downloaded from Bedny and Tian[41], and full details are available at Tian et al.[42]. MRI anatomical and functional images were collected on a 3T Phillips scanner at the F. M. Kirby Research Center. T1-weighted anatomical images were collected using a magnetization-prepared rapid gradient-echo (MP-RAGE) in 150 axial slices with 1 mm isotropic voxels. Resting-state fMRI data were collected in 36 sequential ascending axial slices for 8 minutes. TR = 2 s, TE = 0.03 s, flip angle = 70°, voxel size = 2.4 × 2.4 × 2.5 mm, inter-slice gap = 0.5 mm, (FoV) = 192 x 172.8 x 107.5 mm^3. Participants completed 1 to 4 scans of 240 volumes each (average scan time = 710.4 seconds per person). During the resting state scan, participants were instructed to relax but remain awake. Sighted participants wore light-excluding blindfolds to equalize the light conditions across the groups during the scans.

50 sighted adults and 30 congenitally blind adults contributed the resting state data (sighted: n = 50; 30 females; mean age = 35.33 ± 14.65; mean years of education = 17.08 ± 3.1; blind: n = 30; 19 females; mean age = 44.23 ± 16.41; mean years of education = 17.08 ± 2.11. Blind and sighted participants had no known cognitive or neurological disabilities (screened through self-report). A board-certified radiologist read all adult anatomical images and no gross neurological abnormalities were found. All the blind participants had at most minimal light perception from birth. Blindness was caused by pathology anterior to the optic chiasm (i.e., not due to brain damage). All participants gave written informed consent under a protocol approved by the Institutional Review Board of Johns Hopkins University. The

dataset was made publicly available online after normalizing anatomical and structural data to MNI space, changing the voxel resolution of T1 images to 2 mm^3 and functional images to 2.4 x 2.4 x 3 mm.

2.1.3 Dataset 3

The dataset was collected in Malopolskie Centrum Biotechnologii, Jagiellonian University, Kraków on a 3T Siemens Magnetom scanner. T1-weighted anatomical images were collected using a magnetization-prepared rapid gradient-echo (MP-RAGE) in 1 x 1 x 1 mm voxels. Resting-state fMRI data were collected for 15 minutes. TR = 1.5 s, TE = 0.027 s, flip angle = 90°, voxel size = 3 x 3 x 3.5 mm. During the resting state scan, participants were instructed to relax but remain awake. The study was approved by the ethics committee of the Jagiellonian University. Written informed consent was obtained from all participants before the experiment. Participants were reimbursed for taking part in the study. The participants were screened and had no disability apart from vision loss. The dataset includes 17 congenitally blind participants (mean age: 25.75 ± 5.72, 6 females, 11 males), and is organized in BIDS format.

2.1.4 Dataset curation and quality check

Upon receiving, Dataset 2 was reorganized into BIDS format by a custom script. After an initial visual check, scans with artifacts were removed. Most common artifacts were blurriness due to motion and incomplete slices. At the end, out of 80 participants, 58 participants with single resting-state run (36 sighted and 22 blind individuals) were qualified for further processing. No participants were removed from Datasets 1 and 3 and their full samples (50 and 17, respectively) were used in the preprocessing steps.

2.2 Preprocessing

The datasets were preprocessed with Micapipe[43], an automatic processing pipeline using state-of-the-art software for processing structural and functional MRI data such as AFNI[44], FSL[45], ANTs[46], FreeSurfer[47], FastSurfer[48], and Connectome Workbench (RRID:SCR_008750). Full details of the analysis pipeline can be found at https://micapipe.readthedocs.io/. Briefly, each T1-weighted run was LPI-reoriented, deobliqued, and oriented to standard space (MNI152), a bias-field correction was applied, and the intensity of the images was rescaled between 0-100. Whole-brain, gray matter (GM), white matter (WM), and cerebrospinal fluid (CSF) segmentation was performed. The T1 image was then non-linearly registered to MNI152. Surface meshes in individual spaces were created. Affine registration from fsaverage5 mesh to individual meshes were calculated. Using these registration matrices, the Glasser parcellation[49], which is available in the Micapipe library for the fsaverage5 mesh, was sent to subject space. Using the 360 available regions of interest (ROI) in the Glasser parcellation, regions-wise statistics such as cortical thickness, mean curvature, surface area, sulcal depth, and cortical volume were calculated.

Functional images were reoriented to LPI orientation, and a motion-correction algorithm with 6 parameters (rigid-body) was applied to the time series. The motion-corrected time series were then

projected to the fsnative5 mesh and smoothed with a 10 mm Gaussian kernel. The outputs from Micapipe were further cleaned from nuisance regressors using a custom script written in MATLAB. The 36P strategy without global signal regression that is described in Satterthwaite et al.[50] was adopted to choose the regressors of no interest. Specifically, 6 motion regressors, mean signal from white matter and CSF, their first derivatives, power, and power of the first derivatives were chosen. In addition, mean framewise displacement and a linear trend were added to the model. These regressors were removed from the fMRI data using a multiple linear regression model and the residuals were saved. A band-pass filter between 0.01-0.1 was applied to the residuals.

2.3 Calculating the functional connectivity gradients

For each participant, preprocessed time series on fsaverage5 mesh were parcellated using the Glasser atlas (fsaverage5 version available in the Micapipe library). The averaged time series were then correlated with each other, resulting in 360 x 360 correlation matrices for each participant. The matrices were normalized via Fisher's Z transformation.

Functional connectivity gradients based on normalized correlation matrices were generated as described in Margulies et al.[1] (2016) using the available functions in the BrainSpace MATLAB toolbox [51]. In short, correlation matrices were thresholded to keep the top 10% of the connections. Cosine similarity of the sparse matrices was calculated. A non-linear dimension reduction technique, diffusion mapping, was applied to the similarity matrices with an alpha value of 0.5 for the manifold. This step generated 10 gradient values that explain the functional connectivity profile of each ROI and for each participant. Lastly, Procrustes alignment was used on the gradients to make them comparable. Since diffusion mapping can result in values in the opposite directions, a reference gradient available in BrainStat library[52] was used for alignment, which was calculated with the same parameters on fsaverage5 mesh. This procedure generated "gradient scores" that show the position of each region in the gradient space for the first 10 gradients.

To decrease noise, an inter-subject correlation matrix was calculated based on scores of the first gradient. Participants who showed a smaller Pearson's r than the absolute value of 0.4 were removed from further analyses. The final sample for the group comparisons included 44 sighted and 41 blind participants.

2.4 Statistical analyses

2.4.1 Connectivity gradients across neocortex

After removing the effect of age and sex from the gradient scores via a multiple linear regression model, the residuals were used to compare the differences across the groups of sighted and blind individuals for each ROI via two-sample t-tests. This comparison was repeated for the first three gradients. The results were corrected for multiple comparisons with the false-discovery rate (FDR) with Benjamini-Hochberg procedure at $p = 0.05$. Following the region-wise comparison of the gradient scores, the gradient range

(the maximum value minus the minimum value) was compared between groups using a multiple linear regression model where age and sex were included as regressors of no interest. In addition, the explained variances of the gradients and the variance of the gradient scores were compared between groups of blind and sighted individuals with a two-sample t-test. Effects of age and sex on the gradient range, variance, and explained variance were accounted for using a linear regression before applying a t-test.

2.4.2. Community based profiles

To summarise the findings of the ROI analyses, we conducted a network-based z-score analysis of gradient scores for each of the first three gradients. To this end, mean gradient scores of each network were compared between the groups of blind and sighted individuals with two-sample t-tests with multiple comparison correction at a false discovery level of 0.05 (pFDR < 0.05). In addition, we assessed potential differences between the groups in the functional distance between established functional networks[53]. Between-network functional distance was calculated as the distance between network medians. Given that we expected that most of the changes between the two groups would be observed with respect to the visual network, we focused our analyses on the differences in functional distance between the visual network and the rest of the networks.

We used R[54] and afex[55] to perform a linear mixed effects analysis on the network distances. Separate models were run for each of the three first gradients. As fixed effects we entered group (blind vs sighted) and network (SMN, DAN, VAN, LIN, FPN, DMN), as well as their interaction terms into the linear mixed model (LMM). In addition, age and sex were added as fixed effects into the model. As random effects, we had intercepts for participants. P-values for fixed effects were obtained with the Satterthwaite method and were considered significant at $p < .05$. Post-hoc comparisons of significant interactions were conducted using approximate z-tests on the estimated marginal means (EMMs) using the emmeans package[56]. The resulting p-values were corrected for multiple comparisons following the procedure proposed by Holm (1979).

2.4.3 Representation of the early visual areas in the gradient space

To test whether the functional organization in the gradient space reflects the hierarchy of the visual areas, and whether this representation is different in the blind group, the position of the early visual areas within the first three gradients was checked in terms of their ranking.

Our first aim was to see if the median ranks of the early visual areas reflect the functional hierarchy from V1 to V4 in the sighted and blind groups. Group-level median scores were calculated using the mean gradient scores over the four early visual areas for both groups, and the median ranks were ordered from lowest to highest, and their ranking in this order (1 for the lowest value, 4 for the highest value). For each early visual area, a number between 1 and 4 was appointed after this step depending on their gradient score. In order to validate the group-level median ranks, a bootstrap resampling approach was employed. 10000 bootstrap replicates were generated by randomly sampling participants with replacement. For each bootstrap sample, the median values for each visual region for sighted and blind groups were computed. The ranks of median values were then ranked in ascending order, with ranks

assigned from 1 (lowest median) to 4 (highest median). These rank combinations were recorded for each bootstrap replicate. The frequency of unique rank patterns (e.g., “V1-V2-V3-V4”) was counted to determine the most common configurations across bootstrap samples. This approach revealed the distribution of the rank order patterns across the bootstrap sample.

The bootstrap approach highlights the variance across the resampled sample’s medians. To be more specific to our sample, subject-specific rank orders were also calculated. The frequency distribution of 24 possible rankings was compared via a Chi-square test for independence. Observed counts were compared with the expected counts under the null hypothesis that both groups exhibited the same distribution of ranking orders. This analysis was useful to compare the overall ranking order frequency between groups. To test the difference of a specific ranking order (“V1-V2-V3-V4”, that reflects the expected canonical order of early visual areas) a post-hoc analysis was performed by manually examining ranking orders via a separate Chi-square test.

2.4.4 Connectivity gradients within visual areas

Connectivity gradients within visual areas were calculated separately to define the functional organization within the visual cortex and how this organization differs in the blind group. Since the number of ROIs marked as "Visual" in the Glasser atlas is relatively low (26 unique regions), functional connectivity gradients were calculated vertex-wise. The vertices that correspond to "visual" areas according to Glasser areas were chosen in fsaverage5 mesh (Supplementary Figure 2). The selected vertices correspond to 2527 vertices out of 20484 that are available on fsaverage5 mesh. For each participant, preprocessed time series from those vertices were extracted and correlated with each other, resulting in 2527 x 2527 correlation matrices. The matrices were later normalized via Fisher’s Z transformation.

The mean correlation matrix of the sighted group was used to obtain the reference gradients that were used to align the individual gradients. The reference gradient and the individual gradients were calculated using the same method and parameters that were used to calculate whole-brain connectivity gradients (see Section 2.3). After calculating the gradient scores for each vertex, the age and sex effects are removed using a linear regression model, and the residuals are compared between sighted and blind groups via a two-sample t-test.

To assess functional similarity of early visual regions, we compared the minimum functional distance among regions of the functional distance. Therefore, the closer a region is to other regions, the higher functional similarity it represents. We used R[54] and afex[55] to perform a linear mixed effects analysis on the minimum distances. As fixed effects we entered group (blind vs sighted) and ROI (V1, V2, V3, V4), as well as their interaction terms into the linear mixed model (LMM). As random effects, we had intercepts for participants. P-values for fixed effects were obtained with the Satterthwaite method and were considered significant at $p < .05$. Post-hoc comparisons of significant interactions were conducted using approximate z-tests on the estimated marginal means (EMMs) using the emmeans package[56]. The resulting p-values were corrected for multiple comparisons following the procedure proposed by Holm (1979). Preliminary analyses of minimum distances and visual inspection of q-q plots of the residuals

indicated deviations from normality. Thus, minimum distances were log transformed (log(minimum distance)) which led to a roughly normal distribution of the residuals.

2.4.5 Structure-function coupling

For each participant, mean cortical thickness, curvature, sulcal depth, surface area, and volume of each 360 ROIs were extracted. To decrease the dimension of the data and account for all these structural measures at once, a principal component analysis (PCA) was applied to these five measures, and the first component was saved. This step created one structural component per participant.

Inter-subject correlation matrix on the structural component showed distinct similarity patterns across the three datasets, indicating a strong effect of the scanning site on the data. Therefore, the ComBat method, which is specifically designed for adjusting the data for the effect of scanning sites[57–59] was used on the structural component through a publicly available Matlab toolbox (https://github.com/Jfortin1/ComBatHarmonization). Since Dataset 3 consists of congenitally blind participants only, it was not included in this step as data harmonization across sites requires balanced samples from two groups. After removing the participants from Dataset 3, 44 sighted and 27 congenitally participants remained in the pooled dataset. In addition to the site effects, the structural component was also corrected for age and sex during the same step.

A measure of structure-function coupling was calculated using Spearman's rho rank correlation between the structural component and the gradient values for each ROI across sighted or blind participants. The structural component and the gradient values were previously corrected for age and sex. These resulted in two different structure-function coupling maps, for the sighted and blind groups respectively. For each group i and ROI j, the significance of the coupling measure ρ_i^j was obtained by Fischer-Z transforming the values,

$$z_i^j = \frac{1}{2} log\left(\frac{1+\rho_i^j}{1-\rho_i^j}\right),$$

which are distributed according to a normal distribution. From the probability convolution theorem, it follows that the standardized structure-function coupling difference,

$$z_i^{diff} = \frac{z_i^{blind} - z_i^{sighted}}{\sqrt{\frac{1}{n^{blind}-3} + \frac{1}{n^{sighted}-3}}},$$

follows a standard Gaussian distribution. n^{blind} and $n^{sighted}$ are the number of subjects in each group. Then, the two-sided p-value can be easily calculated and FDR corrected using common statistical procedures. In addition to the ROI-wise comparison of the coupling values, coupling strength across the whole cortex was calculated. We defined the coupling strength as the mean absolute coupling value across the whole cortex. Mean absolute coupling values across gradients and both groups were compared via a two-way ANOVA.

In addition to the whole-brain ROI-based calculation of structure-function coupling, vertex-wise structure-function coupling within visual areas was calculated. The aim was to complement the vertex-wise gradient analysis within visual areas. First, PCA was applied to the five structural measures (vertex-wise cortical thickness, curvature, surface area, volume, and sulcal depth) to create a common structural component (see above). The effect of the scanning site was adjusted for at this step using the Combat method[57], and age and sex were included as covariates of no interest. Since Combat requires balanced samples from each site, Dataset 3 was removed from the analysis because it consisted of blind participants only. Each participant's gradient value (after regressing out the effects of age and sex via linear regression) and the structural component were correlated with Spearman's rank correlation within V1, V2, V3, and V4. At the end of this step, each participant had a correlation value for each ROI. The correlation values were compared between sighted and blind groups for each ROI and gradient following the same procedure described in above.

3 - Results

3.1 Demographics

The groups did not significantly differ in age (number of blind participants = 41, mean age = 36.71 ± 14.46, number of sighted participants = 44, mean age = 36.73 ± 13.79; $t(83) = 0.004$, $p = 0.996$) or sex distribution (blind = 21 male/20 female, sighted = 20 male/24 female; $X^2 = 2.28$, $p = 0.595$).

3.2 Connectivity gradients across neocortex

Functional connectivity gradients revealed a canonical functional similarity profile of the cortical regions. The principal gradient G1 showed that brain activity is maximally organized between the unimodal/transmodal cortices. The second axis, G2, showed the visual and sensorimotor/auditory regions, and G3 showed the axis between the frontoparietal control network (FPN) and the rest of the brain (Figure 1; see also, Supplementary Figure 1). On average, the first three gradients (G1, G2, G3) explained 59.68 % of the total variance for both groups (32.01% ± 0.07, 17.23% ± 0.03, and 10.45% ± 0.02, respectively). There were no differences in the explained variance of the gradients between the two groups (explained variances for each gradient were compared via a two-sample t-test, $p > 0.05$ for 3 gradients, corrected with FDR).

Region-wise comparisons of the gradient scores showed that in all three gradients, the groups of blind and sighted individuals significantly differed within visual regions (Figure 1D-F). In G1, the group of blind individuals had higher gradient scores in predominantly early, ventral, and lateral visual areas, suggesting that those areas are less segregated from transmodal areas in blind individuals (Table S1 and S4). In addition, we observed lower gradient scores for G1 in several regions of the SMN, the DAN and the VAN in blind individuals, suggesting that the SMN and the DAN are more segregated from transmodal areas in blind individuals than in sighted controls. In G2, the group of blind individuals had lower gradient scores

in predominantly early and ventral visual areas and higher gradient scores in the SMN, suggesting that in blind individuals early and ventral visual regions are more segregated from the SMN than in sighted controls (Table S2 and S4). In G3, blind individuals had lower scores in predominantly early, dorsal, and lateral visual areas than sighted controls, suggesting that these regions are closer to the FPN in blind individuals (Table S3 and S4). Overall, the functional profile of early, ventral, and lateral visual areas of blind individuals becomes more similar to that of higher-order regions, and the distinction between visual areas and sensorimotor areas is increased. Moreover, early, dorsal and lateral visual areas of blind individuals seem to become more functionally similar to the FPN. In addition, sensorimotor areas shifted away from the origin of the gradient axis in G2 in blind individuals, similar to what has been observed for visual regions.

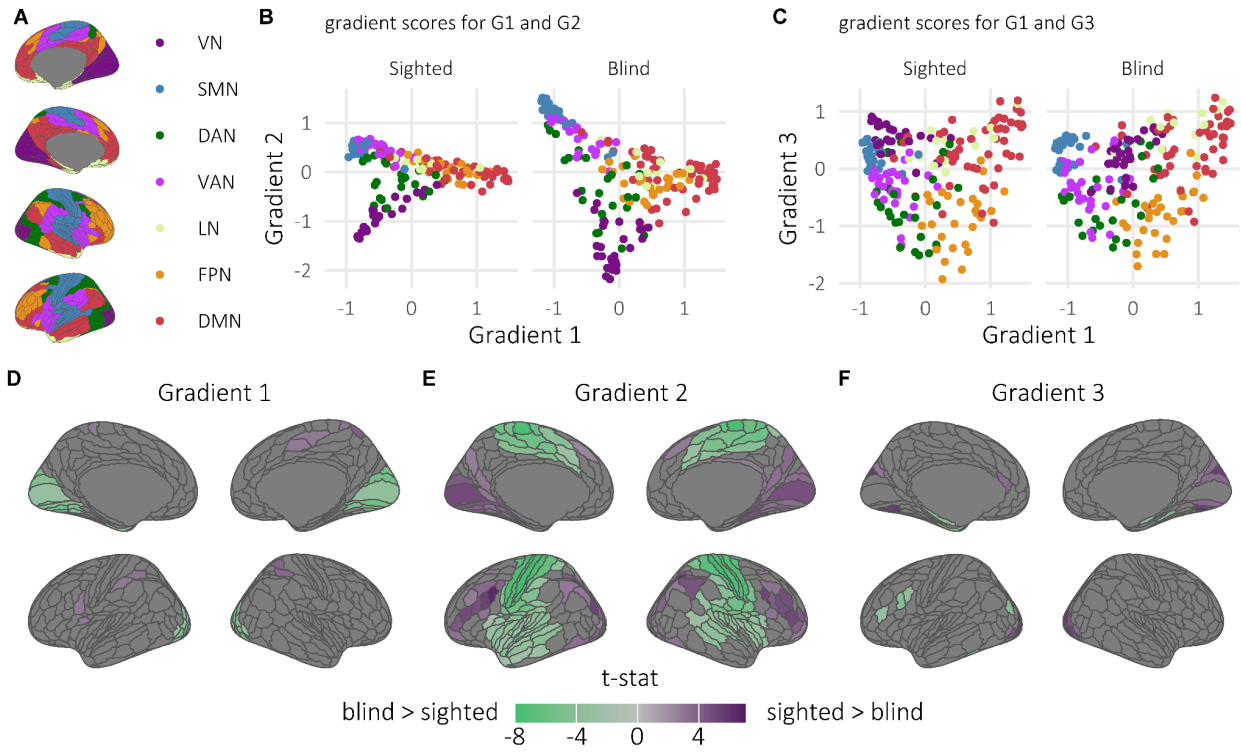

Figure 1: Differences in macroscale functional organization between blind and sighted individuals. A Projection of 7 functional networks defined by Yeo et al.[53] on ROIs defined by Glasser et al.[49] **B - C** Distribution of gradient values across G1 and G2 and across G1 and G3 in the groups of blind and sighted individuals. **D-E-F**: Results of the region-wise comparison of the gradient scores between groups of SC and blind individuals (results were corrected for multiple comparisons with FDR at $p < 0.05$). VN = visual network; SMN = somatosensory/ motor network; DAN = dorsal attention network; VAN = ventral attention network; LIN = limbic network; FPN = frontoparietal network; DMN = default mode network

To summarise the findings from the ROI analysis, we applied a well-established functional community decomposition[53]. Then we conducted a network-based z-score analysis of gradient scores for each of the first three gradients. This analysis revealed that in the first gradient, blind individuals had higher gradient (i.e. less negative) scores in the VN than sighted controls ($t(51.499) = 3.897$, $p < 0.001$) and higher

gradient scores (more positive) in the SMN ($t(51.925) = -4.943$, $p = 0.001$) and VAN ($t(51.116) = 2.693$, $p = 0.022$, Figure 2A, see Table S5 in supplementary material for parameter estimates and confidence intervals). In G2, the group of blind individuals had lower gradient scores in the VN ($t(49.015) = 5.446$, $p< 0.001$, Figure 2B) and the FPN ($t(39.347) = 4.759$, $p < 0.001$) than the group of sighted controls and higher gradient scores in the SMN ($t(42.367) = -12.791$, $p < 0.001$) and the VAN ($t(36.324) = -4.889$, $p < 0.001$). Moreover, in G3 we observed that the group of blind individuals had lower gradient scores in the VN ($t(52.754) = 3.999$, $p < 0.001$, Figure 2C) than sighted controls.

In the next step, we tested for potential group differences in the distance of the VN and the rest of the networks. In G1, the VN of blind individuals showed a greater distance to the SMN and the VAN compared to sighted controls (group x network interaction: $F(6, 498.00) = 19.24$, $p < 0.001$, Figure 2A, see Table S6 and S7 for results of the post-hoc tests and EMMs), whereas the FPN and DMN were closer to the VN in blind individuals than in sighted controls. In G2, the VN of blind individuals was further removed from the SMN, DAN, VAN, FPN, LN, and the DMN than the VN of sighted controls (group x network interaction: $F(6, 498.00) = 17.27$, $p < 0.001$, Figure 2B, see Table S8 and S9 for results of the post-hoc tests and EMMs). In G3, the VN of blind individuals was closer to the DAN, VAN, and FPN than the VN of sighted controls (group x network interaction: $F(6, 498.00) = 11.23$, $p < 0.001$, Figure 2C, see Table S10 and S11 for results of the post-hoc tests and EMMs), whereas the VN of blind individuals showed greater distance to the LN than the VN of sighted individuals.

The gradient range of G2 (defined as the maximum value of G2 minus the minimum value of G2) was higher in blind individuals ($t(83) = 4.81$, $p < 0.001$). No differences in gradient range between the groups were observed in G1 and G3 (all $p > 0.05$). Although the gradient range was related to the explained variance for both groups (Spearman's Rho between gradient range and explained variance for G1: 0.85, G2: 0.43, G3: 0.26), the explained variances did not significantly differ between the groups of sighted and blind individuals (all ps > 0.05). Another variable correlated with gradient range for both groups was gradient variance (correlation between G1 range and variance: 0.96, G2: 0.93, G3: 0.91). Here, we observed that the variance of G2 was higher in blind individuals compared to sighted controls ($t(83)$: 4.21, $p < 0.001$).

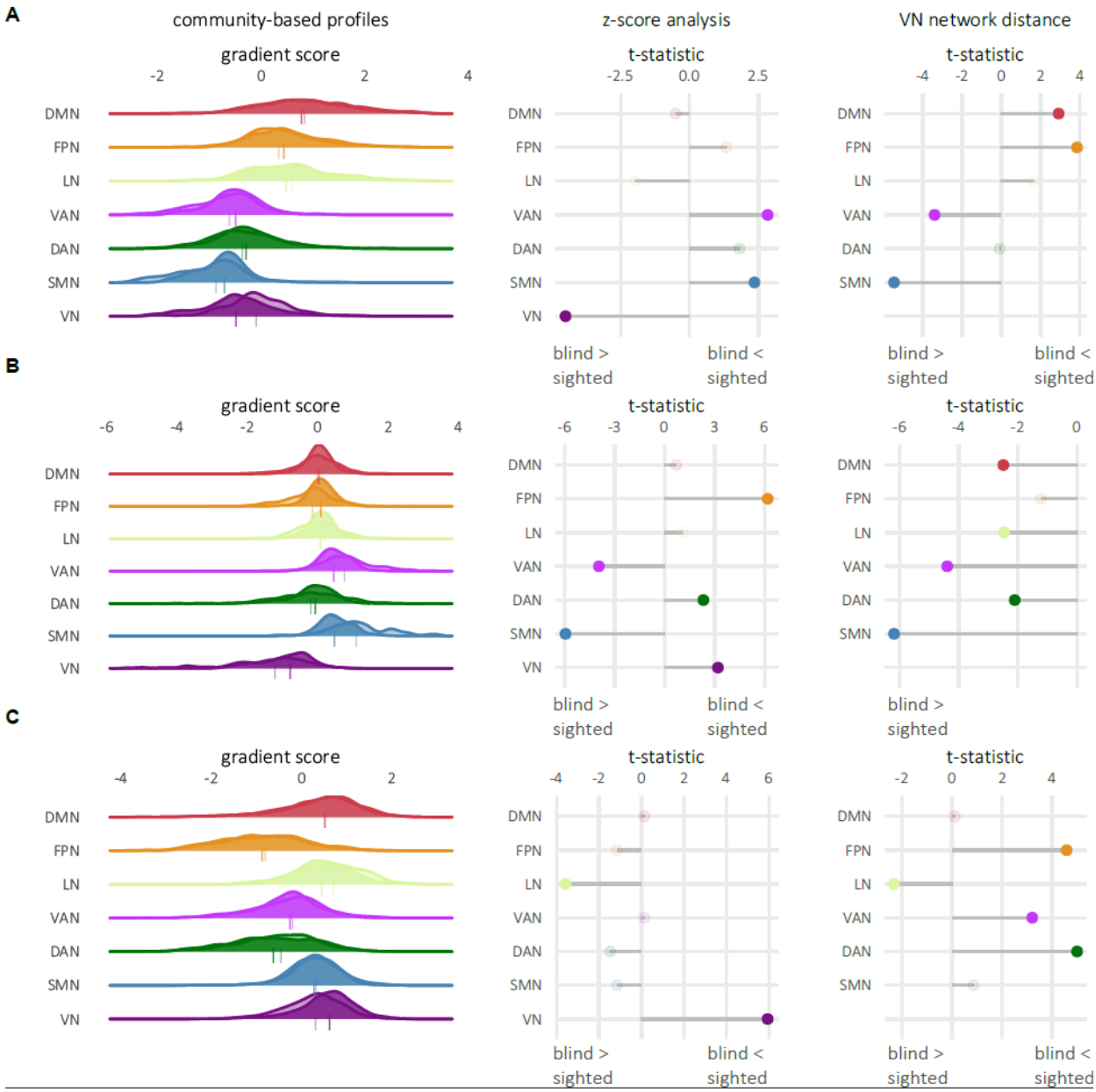

Figure 2: Differences in community based profiles between the groups of blind and sighted individuals. A-B-C left panel: Distribution of the gradient scores for each of the 7 functional networks (transparent distribution: group of blind individuals, non-transparent distribution: group of sighted controls). The tick below the density plots represents the mean gradient score. **A-B-C middle panel**: Group differences in the mean gradient scores across 7 functional networks. Significant differences are shown with full color, whereas non-significant differences are shown with transparent color. **A-B-C right panel**: Group differences in the distance between the VN and other functional networks. Significant differences are shown with full color, whereas non-significant differences are shown with transparent color. VN = visual network; SMN = somatosensory/ motor network; DAN = dorsal attention network; VAN = ventral attention network; LIN = limbic network; FPN = frontoparietal network; DMN = default mode network.

3.3 Representation of the early visual areas in the gradient space

In sighted controls, the median ranking of the EVC in G1 showed the canonical "V1-V2-V3-V4" order 4265 times out of 10000 bootstrapped samples. This linear ranking order from V1 to V4 was not as frequent in the blind group (514 times out of 10000, Figure 3B, Table S12). For G2, both groups showed the "V1-V2-V3-V4" order as the most common one (6147 times for sighted controls, 5540 times for blind individuals, Figure 3B, Table S12). Lastly, for G3, the sighted group showed a relatively uniform distribution, having "V4-V3-V2-V1" order as the most common one (2334 times), whereas the blind group showed a dominant distribution for "V2-V1-V3-V4" order 6942 times (Figure 3B, Table S12). The complete details of the distribution are available in Table S12. These distributions imply that a linear order in the gradient space of G1 from V1 to V4 is available in sighted individuals, but not in blind individuals. The canonical order remains largely unaltered in the G2 axis.

In addition to bootstrapping, which enables us to inspect the most common ranking order estimate by resampling the dataset, we also directly compared the distributions and frequencies of different orders across the two groups without bootstrapping. Subject-wise rank orders showed different distributions across sighted and blind groups for all three gradients (G1: $X^2 = 19.01$ $p < 0.001$; G2: $X^2 = 22.41$ $p < 0.001$; G3 $X^2 = 27.69$ $p = < 0.001$). In G1, post-hoc comparison showed that the frequency of the canonical order ("V1-V2-V3-V4") is different between the two groups (occurrence in the sighted group: 14, occurrence in the blind group: 7; $X^2 = 17.19$, $p < 0.001$). This finding is similar for G2 (occurrence in the sighted group: 18, occurrence in the blind group: 10; $X^2 = 24.14$, $p < 0.001$). In the blind group, the occurrence of the linear order in G2 at the subject-level shows a different pattern than that of sample-level (results of the bootstrapping). In G2, bootstrapping results indicate an intact canonical order, whereas the subject-level distribution shows that this order may not be as common in blind as in sighted individuals. Nonetheless, this reduction in occurrence could be attributed to a larger variability of the blind group rather than an inherent alteration of the hierarchical processing. Lastly, for G3, consistent with the bootstrapping results, the most common ranking order for the sighted group was "V4-V3-V2-V1" (12 times), and for the blind group "V2-V1-V3-V4" (16 times). A complete list of the distributions is available in Table S13.

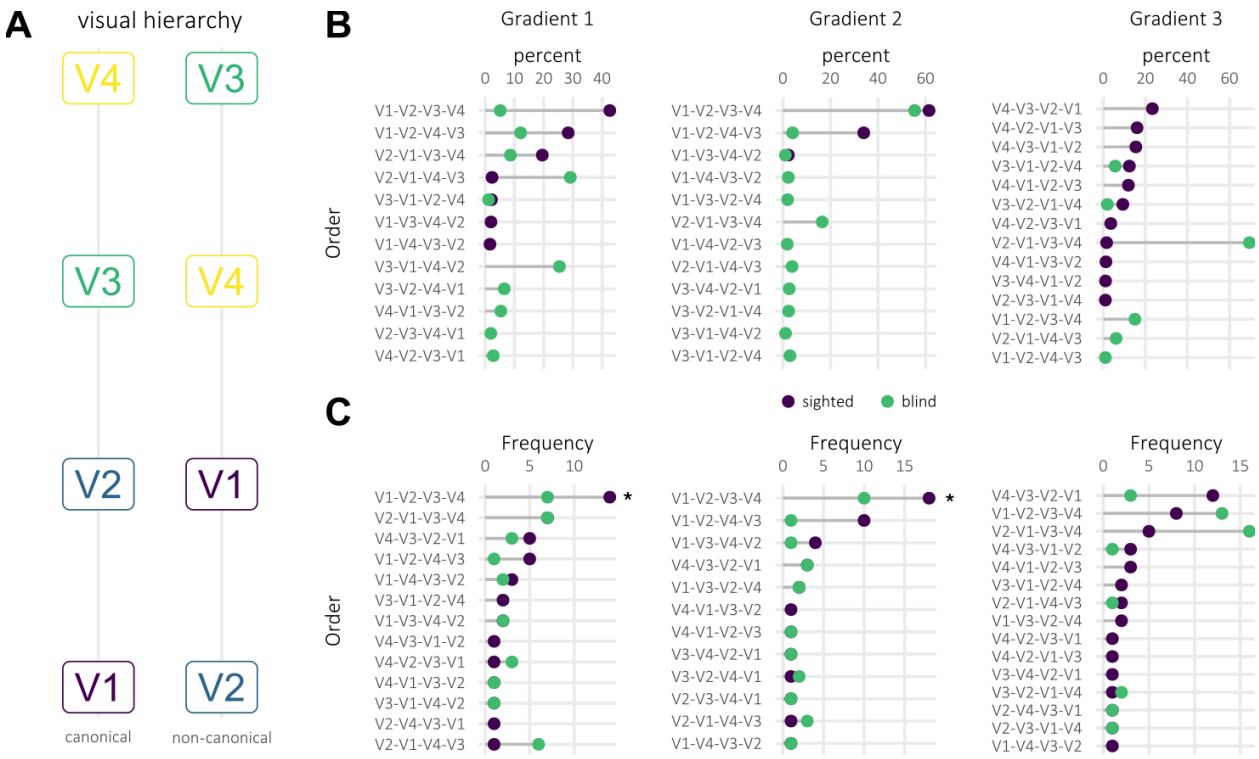

Figure 3: Differences in hierarchical organisation of the early visual cortex between congenitally blind individuals and sighted controls. A Hypothetical canonical and non-canonical hierarchy of the early visual cortex. **B** Percent distribution of the ranking orders across groups and gradients after bootstrapping. The bootstrapped samples showed "V1-V2-V3-V4" ranking order within early visual areas for the first two gradients. Only ranking orders with percent > 1 are displayed. **C** Frequency distribution of the ranking orders without bootstrapping. The canonical "V1-V2-V3-V4" distribution showed significant group differences for both G1 and G2 ($p < 0.05$, marked with asterisk).

3.4 Connectivity gradients within visual areas

The first three connectivity gradients within visual areas explained 49% of the variance in sighted controls (27.68% ± 10.33, 11.64% ± 2.52, 7.67% ± 1.94 for G1, G2, and G3 respectively). In blind individuals, G1 did not show any difference compared to that of sighted controls (explained variance: 27.11 8.28, t(83): -0.31, p = 0.756), but G2 (explained variance: 15.14 3.73, t(83): 5.16, p = 0.001) and G3 (explained variance: 8.94 2.01, t(83): 2.91, p = 0.004) showed a higher explained variance in blind individuals. In G1, the connectivity within visual areas is mainly organized between V1 and lateral occipital areas in sighted individuals. In this axis, blind individuals showed lower gradient scores in V1, specifically in the occipital pole, and higher values in MT+ (Figure 4A). This could suggest different functional clustering of early visual areas in blind compared to sighted individuals. G2 is organized along the posterior-anterior axis. In G2, the group of blind individuals had lower values in the dorsal stream and MT+. Lastly, G3 shows an organization between MT+ and the dorsal stream. Scores of the blind group increased in the dorsal stream and decreased in V1 (Figure 4A). The decomposition of the gradient

scores by regions can be found in Supplementary Figure 3. Apart from the vertex-wise gradient scores, the groups of blind and sighted individuals also differed in gradient range and variance in gradient scores in G2, but not in G1 and G3.

To summarise the findings from the vertex-wise analysis, we additionally assessed the minimal functional distance of each early visual area (V1, V2, V3, V4) and the rest of the early visual areas. No significant group differences in log(minimum distance) were observed in G1 (Figure 4B, Table S14 and Table S15). In G2, the group of sighted individuals had a greater log(minimum distance) for V1 than the group of blind individuals (group x ROI interaction: ($F(3, 249.00) = 4.52$, $p = 0.004$, see Table S16 for the EMMs (non-transformed data for ease of interpretability) and Table S17 for the post-hoc tests (performed on the log scale), and Figure 4B). This suggests that in G2, V1 is more functionally distinct from the other areas of the EVC (V2, V3, V4) in sighted controls than blind individuals. In G3, the group of blind individuals had a greater log(minimum distance) for V3 and V4 than the group of sighted individuals (group x ROI interaction: ($F(3, 249.00) = 9.66$, $p < 0.001$, see Table S18 for the EMMs and Table S19 for the post-hoc tests). This suggests that in G3, V3 and V4 are more functionally distinct from V1 and V2 in blind individuals than in sighted controls.

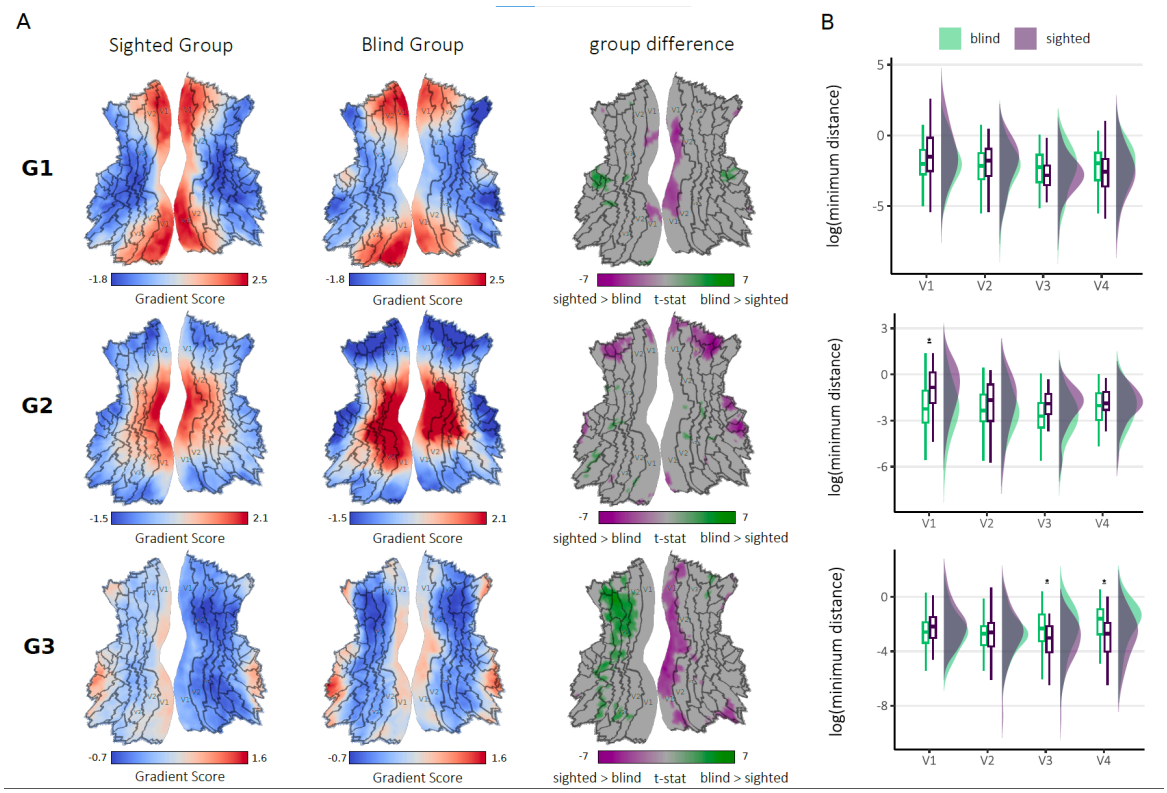

Figure 4: A Functional organization within visual areas. G1 shows that functional organization in visual areas is mainly defined by the functions from V1/V2 to the rest of the visual areas. G2 is shaped around the anterior-posterior axis, and G3 is organized within the dorsal stream. **B** Minimum functional distance to the rest of the early visual regions.

3.5 Structure-function coupling

The principal structural component created for each participant using their cortical thickness, volume, surface area, sulcal depth, and curvature explained 98.43% ± 0.41 of variance. Region-wise comparison between the structural component scores of the groups of sighted controls and blind individuals did not show any significant differences after correction for multiple comparisons. However, non-corrected p-values indicated that the group of blind individuals had lower structural scores in visual and sensorimotor areas, and higher scores in higher-order areas (Supplementary Figure 5B).

In G1, the coupling between G1 and the structural component resembles the pattern of G1 itself, indicating a strong underlying structural mechanism for functional organization. Mean absolute coupling values across gradients and both groups were compared via a two-way ANOVA. The ANOVA model revealed a significant interaction between the group and gradient ($F(2,2154) = 63.62$, $p < 0.001$, Table S20). Tukey-kramer post-hoc tests revealed that G1's mean absolute coupling value was significantly higher in sighted controls than in blind individuals (mean absolute coupling value of sighted group = 0.31 ± 0.16, of blind group = 0.19 ± 0.13, estimated value of difference (EVD) = 0.11, $p < 0.001$, Figure 5C). A complete list of EVDs can be found in Table S21. When the coupling values for G1 in each ROI were compared between groups, visual (Figure 5B, regions colored with purple) and middle temporal areas (Figure 5B, regions colored in green, $p < 0.05$, corrected with FDR across whole-brain) showed a stronger coupling in the group of sighted controls (Table S22).

Tukey-Kramer post-hoc test following the ANOVA model above revealed that in sighted controls, the coupling between G2 and the structural component showed a similar pattern to G2 itself, that is, a positive coupling in sensorimotor areas and a negative coupling in visual areas (mean absolute coupling value: 0.10 ± 0.07). However, compared to G1, overall coupling strength decreased significantly, indicating a weaker coupling mechanism for G2 (EVD = 0.21, $p < 0.001$, Table S21). These results indicate considerable but weaker structure-function coupling in G2 for the sighted control group compared to G1. By contrast, for the blind group, the coupling strength did not significantly differ between G1 and G2 (mean absolute coupling value for G1: 0.19 ± 0.13, for G2: 0.17 ± 0.11, EVD = 0.02, $p = 0.188$, Table S21). A significant difference was observed in mean absolute structure-function coupling in G2 between blind individuals and sighted controls (mean absolute coupling value of sighted group = 0.10 ± 0.07, of blind group = 0.17 ± 0.11, EVD = -0.07, $p = < 0.001$, Table S21). Lastly, ROI-wise comparisons of the coupling values between sighted and blind groups did not reveal any significant differences.

The mean absolute coupling value in G3 for the sighted group was 0.11 ± 0.09, and 0.13 ± 0.10 for the blind group. Compared to G1, the overall coupling strength decreased significantly, indicating a weaker coupling mechanism for G3 (EVD = 0.201, $p < 0.001$, Table S21). No significant differences between groups were observed in the mean absolute structure-function coupling in G3 (sighted group = 0.11 ± 0.09, blind group = 0.13 ± 0.10, EVD = -0.01, $p = 0.247$, Table S21), nor in the ROI-wise comparisons.

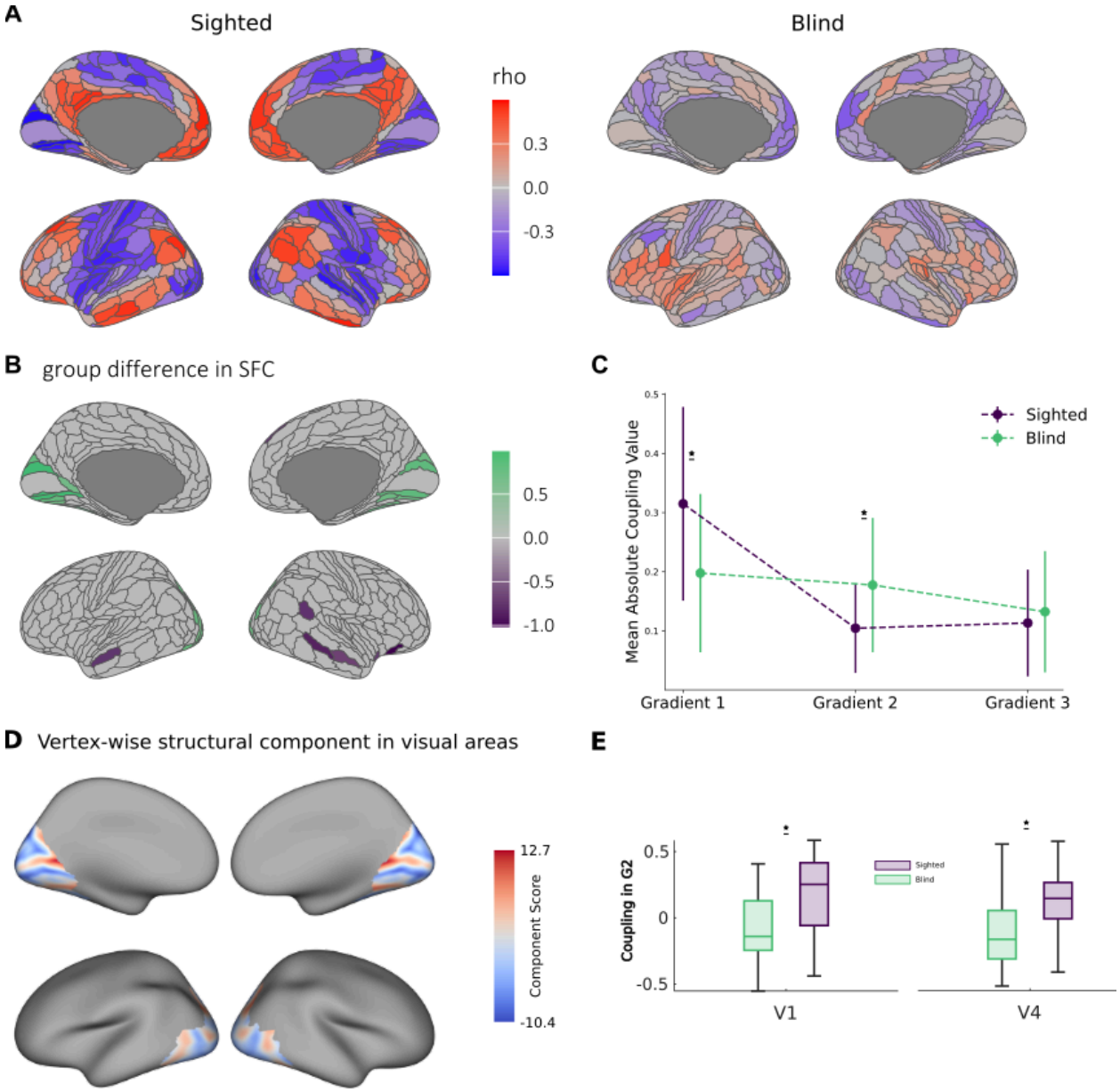

Figure 5 | Correlation between G1 values and the structural components across groups. A Structure-function coupling values for groups of sighted controls and blind individuals. **B** Decreased structure-function coupling for G1 in the group of blind individuals in visual and temporal areas. **C** Comparison of the mean absolute coupling value across gradients and groups. The mean absolute coupling value derived from the coupling maps indicates the strength of the coupling across the cortex. The group of blind individuals shows weaker coupling with G1 and stronger coupling with G2. **E** Vertex-wise structural component within visual areas. **E** Correlation between the structural component shown in Panel D and mean coupling with G2 in V1 and V4 across two groups. The group of blind individuals showed less structure-function coupling compared to the group of sighted controls.

The structural component explains 94.56% ± 1.41 of the variance across vertex-wise cortical thickness that covers the visual areas only, volume, sulcal depth, surface area, and curvature. Since it was calculated on the vertex level, unlike the ROI-based component, it shows finer structural details, such as sulci and gyri (Figure 5D). The coupling between the structural component and the gradient scores across V1, V2, V3, and V4 showed that V1 and V4 have a decreased coupling with G2 for the blind group (mean V1-G2 coupling in sighted group: 0.16, 0.3, blind group: -0.08 ± 0.26, $t(69): 3.65$, $p < 0.001$; mean V4-G2 coupling in sighted group: 0.13 ± 0.2, in blind group: -0.08 ± 0.24, $t(69): 3.95$, $p < 0.001$, Figure 5E, correlations of every ROI with ever gradient can be found in Supplementary Figure 4).

4 - Discussion

One of the main principles of human brain organization is the hierarchical arrangement within and between cortical networks. This hierarchical organization guides the flow of information and allows higher-order areas to process transmodal information that is unrelated to immediate sensory input[1,60]. Here, we aimed to investigate to what extent this hierarchical organization is an innate feature of human brain organization and to what extent it depends on sensory input during development. To this end, we compared functional connectivity gradients and their relationship to structural measurements between blind individuals and sighted controls. Both groups showed a principal gradient (G1) that extended from unimodal to transmodal areas, a second gradient (G2) that extended from somatosensory to visual areas, as well as a third gradient (G3) that extended between the FPN and the rest of the brain. However, compared to the sighted group, the visual network was more distanced from the sensorimotor network in G2, while it was more integrated with transmodal networks in G1 and frontoparietal networks in G3. Additionally, we observed that the hierarchy and the functional connectome within the early visual cortex were altered in the group of blind individuals. Within the first three gradients, we observed marked differences in the functional clustering of visual areas, suggesting that visual input plays a critical role in areal specialisation. Our results also indicate reduced structure-function coupling in visual and temporal regions for G1 in blind individuals. Taken together, the results of this study suggest that the broad macroscale organization of the brain develops independently of sensory experience and that visual experience is essential for refining a presumably innate functional hierarchical organization within and between cortical networks.

Connectivity gradients across the neocortex

Previously, it has been suggested that the hierarchical organization of the cortex is necessary for sensory signals to be transformed into more abstract representations[1,2]. In blind individuals, we observed a reduced functional segregation between early, ventral, and lateral visual areas and transmodal areas, along with a concomitant increase in functional segregation between early and ventral visual regions and sensorimotor areas. Previous research indicates that blind individuals engage early, ventral, and lateral visual areas during spoken language processing[3,16,61,62]. Crucially, responses to language in these areas have been shown to be modulated by grammatical complexity and semantic content of the stimuli, with activity being greater for stimuli that have meaning and grammatical structure[3,5,61,62]. These findings

provide evidence for the notion that information processed by visual cortices of blind individuals during language tasks is symbolic and abstract, rather than sensory[63].

It could be argued that the visual cortices can take on these new higher-level functions and process abstract information because of their functional distance to other networks. In fact, there is now emerging consensus that the role of the higher-level regions in cognition relates to their physical and functional distance from the sensory and motor systems[1,64]. For example, the DMN exhibits the greatest physical and functional distance along the cortical surface and is equidistant from primary sensory and motor areas[1]. This topographical organization is thought to enable the processing of supramodal information that is independent of immediate sensory input[1,2,64]. Similarly, it could be argued that the increased functional segregation between early and ventral visual regions and regions of the SMN in blind individuals is a necessary prerequisite for the processing of abstract (linguistic) information in these regions.

In the third gradient, we observed a reduced functional segregation between a network of early visual (V3 and V4) and predominantly dorsal visual areas and the FPN. The FPN is thought to play a central role in cognitive control by coordinating task demands and goals, and by modulating processing in other brain regions through top-down mechanisms[65,66]. It has been suggested that the FPN may gain its multiple demand ability by flexibly interacting with a variety of functionally specialized brain networks[66,67]. This adaptive regulation allows for the efficient implementation of task requirements across different cognitive domains[65,67]. Similarly, the visual cortices of blind individuals have been shown to play a role in a number of different cognitive domains, including working memory and cognitive control, and to interact with functionally specialized networks across the brain[4,5,17,63,68]. Based on this, it could be hypothesized that dorsal visual cortices of blind individuals become part of the FPN[39].

Overall it seems like dorsal visual regions become functionally more similar to the FPN, while the early visual (V1 and V2) and ventral visual areas become functionally more similar to other transmodal areas. This is not only supported by our findings in the first and third gradient, but also by the finding that mostly early and ventral visual areas seem to be more functionally distinct from regions of the SMN than dorsal areas. This latter finding is consistent with previous studies that have reported greater decrease in rsFC between S1 and early and ventral visual regions in blind individuals, compared to dorsal visual regions[69]. Thus, it seems like a functional segregation between dorsal and ventral visual areas is retained in blind individuals. Indeed, early (V1 and V2) and ventral “visual stream” areas in blind individuals have been associated with language[3], reading[16], and object recognition[70], whereas dorsal “visual stream” regions have been associated with the processing of auditory motion[71] and numerical cognition[17]. Moreover, in blind individuals, activity of number-responsive visual areas has been shown to be correlated at rest with frontoparietal number areas, whereas language responsive regions of visual cortex are correlated with prefrontal language regions[17,42].

Altered hierarchy within early visual areas of congenitally blind individuals

Previous studies have shown that there is a close correspondence between functional gradients and functional hierarchies[1,72]. However, whether the functional organization in gradient space reflects the hierarchy of the visual areas has not been tested. To this end, we assessed the position of the early visual areas within the first three gradients in terms of their ranking. In G1, the group of sighted controls showed a very consistent linear order of V1-V2-V3-V4, whereas in the blind group the ranking was much less consistent and the most frequent order was V2-V1-V4-V3. These findings suggest that the hierarchy of the early visual cortex in blind individuals is drastically altered and is reminiscent of previous findings of more heterogeneous resting state functional connectivity patterns in blind individuals[73]. Interestingly, in G2, the hierarchy seemed to be more canonical in the group of blind individuals (V1-V2-V3-V4) and simulations suggested that the ordering is similarly consistent between blind and sighted populations. However, when the analysis was specifically done on the non-simulated data, the ranking order of the blind individuals showed less consistency compared to sighted individuals. This difference between the results of simulated and the real data could be another indicator for the heterogeneity in the functional organization of the early visual cortex of blind individuals. In G3, the hierarchy seemed to be reversed in sighted individuals (V4-V3-V2-V1), but much less consistent than in G1 and G2. By contrast, blind individuals showed a very consistent but non-canonical hierarchy in G3 (V2-V1-V3-V4).

Rakic et al.[74] have shown that in enucleated macaques, a novel cytoarchitectonic area emerges between V1 and V2, combining features of both primary visual and extrastriate cortex. This region, also known as the *hybrid cortex*[75], was recently shown to occupy a relatively high position in the cortical hierarchy and to receive enhanced input from ventral stream areas[75]. Although no study has yet identified the development of a novel cytoarchitectonic area in blind humans, it seems plausible that similar mechanisms occur as observed in enucleated macaques in the study by Magrou et al.[75]. Specifically, in the absence of feedforward input to V1, it likely receives reinforced input from higher-order areas, altering its position within the functional hierarchy of the visual cortex. This could also explain the finding that in G2 and G3, V1 was functionally less distinct from the rest of the EVC (V2, V3, and V4) in blind individuals. That is, the lack of feedforward input from the LGN to V1 in blind individuals, could decrease the functional segregation of V1 from the rest of EVC.

Altered functional clustering in congenitally blind individuals

Next, we assessed connectivity gradients within visual areas to further explore potential changes in its functional organization in blind individuals. Previous studies have demonstrated that cortical parcellations based on rsFC gradients closely align with task activation maps and show strong correspondence with probabilistic delineations of V1 and V2[33,34]. Consistent with these findings, we observed a correspondence between the V1-V2 areal borders and G1 in sighted controls. However, in blind individuals, this correspondence was absent at the dorsal border. This finding is consistent with findings from Striem-Amit et al.[4] who compared the connectivity pattern from a seed in V1 with that of a

seed in the same visual field in V2. They reported that while the entire ventral border between V1 and V2 could be constructed using rsFC maps in blind individuals, the dorsal border was not clearly visible[4]. These results suggest that visual input may be necessary for the refinement of areal borders.

Moreover, in blind individuals probabilistic V1 appeared to be split into two distinct functional clusters: the occipital pole exhibited increased functional similarity to ventral occipitotemporal areas, while the rest of V1 formed a cohesive cluster with dorsal V3. By contrast, in sighted controls V1 seemed to form one cohesive functional cluster in G1. Moreover, in G3 of blind individuals, the occipital pole became functionally more integrated with V3 and V4, as well as with lateral visual regions, whereas in sighted controls it was functionally more integrated with the apex of the dorsal and ventral visual stream. Previously, it has been observed that the occipital pole and the rest of V1 are connected to different areas in the frontal cortex in blind individuals: the occipital pole showed increased functional connectivity to the inferior frontal gyrus, particularly in the left hemisphere, whereas the peripheral V1 showed stronger functional connectivity to the dorsolateral prefrontal cortex[4]. These findings provide further evidence for the notion that the lack of visual input during development leads to changes in areal specialization. This dovetails nicely with our findings of a changed hierarchy in blind individuals and the increased functional coupling of the occipital pole with ventral occipitotemporal areas, which has also been observed for the hybrid cortex in enucleated macaques[75]. Considering our findings and the previous reports, it can be assumed that foveal and peripheral V1 are functionally segregated in case of blindness.

Reduced structure-function coupling in congenitally blind individuals

The coupling between G1 and the structural component mirrored the overall pattern of G1, suggesting a robust structural mechanism underlying its functional organization, however, structure-function coupling was reduced in visual and middle temporal areas of blind individuals. Studies that have assessed structure-function coupling using white matter connectivity as a proxy for structure, have reported strong structure-function coupling in ventral and early visual areas as early as 1 and 2 years of age, with continued strengthening up to at least 6 years of age[76]. Other studies that have looked into structure-function coupling using gross morphological measures have also reported a strengthening of structure-function coupling from childhood to adulthood[77]. Taken together, these findings suggest that structure-function coupling within visual areas is already established in early childhood and continues to be strengthened throughout development. Our results suggest that the development of this structure-function coupling is dependent on sensory input during development.

Recent evidence indicates that increased myelination and a lower excitation-inhibition (EI) ratio are linked to more rigid structure-function coupling[78]. While myelination has not yet been investigated in blind individuals, there is indirect evidence to suggest reduced myelination of the occipital cortices of blind individuals. Previous studies have shown that the visual cortices of blind individuals have increased cortical thickness as measured by MRI[11,13,14] which might correspond to lower myelination[79]. Moreover, there is evidence to suggest that the EI ratio is increased in blind individuals[80,81]. Based on these findings,

it could be hypothesised that the reduced structure-function coupling observed in blind individuals, particularly in the visual cortices, may stem from reduced myelination and an increased EI ratio.

This lack of structure-function coupling, particularly in visual regions, in blind individuals could also be the result of applying a uniform parcellation to all participants. This entails the assumption that functional areas can be mapped to identical spatial locations in all participants[82]. However, as we have shown here, the functional organization within visual areas seems to be altered in blind individuals, particularly in early visual regions. Not only did we find evidence for changes of the hierarchical organization, but the results from the connectivity gradients within visual areas suggest that the areal specialization between areas may differ between blind individuals and sighted controls. Thus, structure-function relationships may not be perfectly captured if the areas are not correctly aligned with the functional organization, as seems to be the case in blind individuals. A key challenge for future research on structure-function coupling in sensory deprived individuals is how to reconstruct networks while accounting for individual variations in topographic organization[82]. One possibility could be to create individual cortical area parcellations using rsFC[33,83].

It should be noted that previous studies have reported a tight coupling between structure and function in primary sensory and motor areas, whereas in transmodal association areas, structure and function appeared to diverge[35–38,84]. By contrast, we observed a structure-function coupling axis that showed strong coupling in visual and sensorimotor areas, as well as in transmodal areas, with weaker associations between structure and function in intermediate regions. These divergent results could be explained by the different proxies for structure that have been used in our study, compared to previous studies. Most studies that have looked at structure-function coupling in the macroscale organization of the brain have mostly relied on structural connectivity as a proxy for structure[82], whereas we used a composite derived from a PCA analysis that included mean cortical thickness, curvature, sulcal depth, surface area, and volume. Previous studies have shown a close correspondence between these gross morphological measures and functional specialization. For example, in V1, surface topology is predictive of the underlying retinotopic organization[85]. And even in higher-level visual areas, there seems to be a close correspondence between sulcal folds and functional specialization[86,87]. These findings show that gross morphological measurements are highly suitable for studying structure-function relationships.

Conclusion

Our findings suggest that while the broad macroscale hierarchical organization of the brain develops independently of sensory experience, visual input plays a critical role in refining this organization. The groups of blind and sighted individuals exhibited similar large-scale gradients, indicating an innate framework. However, distinct alterations in both global gradient patterns and functional connectivity within the visual cortex in blind individuals highlight the importance of visual experience in fine-tuning these cortical hierarchies and in refining the borders between functional regions. Our study is the first to demonstrate reduced structure-function coupling in visual and temporal regions, specifically linked to altered gradients in blind individuals. These results underscore the interplay between innate brain organization and sensory-driven refinement, particularly within visual networks.

Data availability

The scripts used in this study are available at https://github.com/KobaCemal/BlindnessGradients and https://github.com/LenaStroh/BlindnessGradients .

Acknowledgements

Research supported by the Polish National Science Centre (NCN) grant no: 2018/30/A/HS6/00595 to M.S. Cemal Koba and Joan Falcó-Roget were supported by the project of the Minister of Science and Higher Education "Support for the activity of Centers of Excellence established in Poland under Horizon 2020" on the basis of the contract number MEiN/2023/DIR/379, and the European Union's Horizon 2020 research and innovation programme under grant agreement No 857533, and by Sano project carried out within the International Research Agendas programme of the Foundation for Polish Science, co-financed by the European Union under the European Regional Development Fund. Cemal Koba and Joan Falcó-Roget gratefully acknowledge Polish high-performance computing infrastructure PLGrid (HPC Center: ACK Cyfronet AGH) for providing computer facilities and support within computational grant no. PLG/2024/017108. Olivier Collignon is a senior researcher at FRS-FNRS in Belgium. We would like to thank all of our participants without whom this research would not have been possible.

References

1. Margulies, D. S. *et al.* Situating the default-mode network along a principal gradient of macroscale cortical organization. *Proc. Natl. Acad. Sci. U.S.A.* **113**, 12574–12579 (2016).
2. Mesulam, M. From sensation to cognition. *Brain* **121**, 1013–1052 (1998).
3. Bedny, M., Pascual-Leone, A., Dodell-Feder, D., Fedorenko, E. & Saxe, R. Language processing in the occipital cortex of congenitally blind adults. *Proceedings of the National Academy of Sciences* **108**, 4429–4434 (2011).
4. Striem-Amit, E. *et al.* Functional connectivity of visual cortex in the blind follows retinotopic organization principles. *Brain* **138**, 1679–1695 (2015).
5. Abboud, S. & Cohen, L. Distinctive Interaction Between Cognitive Networks and the Visual Cortex in Early Blind Individuals. 18 (2019) doi:10.1093/cercor/bhz 006.
6. Butt, O. H., Benson, N. C., Datta, R. & Aguirre, G. K. The Fine-Scale Functional Correlation of Striate Cortex in Sighted and Blind People. *J. Neurosci.* **33**, 16209–16219 (2013).
7. Kanjlia, S., Pant, R. & Bedny, M. *Sensitive Period for Cognitive Repurposing of Human Visual Cortex*. http://biorxiv.org/lookup/doi/10.1101/402321 (2018) doi:10.1101/402321.
8. Liu, Y. *et al.* Whole brain functional connectivity in the early blind. *Brain* **130**, 2085–2096 (2007).
9. Wang, D. *et al.* Altered resting-state network connectivity in congenital blind. *Human Brain Mapping* **35**, 2573–2581 (2014).
10. Bridge, H., Cowey, A., Ragge, N. & Watkins, K. Imaging studies in congenital anophthalmia reveal preservation of brain architecture in 'visual' cortex. *Brain* **132**, 3467–3480 (2009).
11. Jiang, J. *et al.* Thick Visual Cortex in the Early Blind. *Journal of Neuroscience* **29**, 2205–2211 (2009).
12. Park, H.-J., Lee, J. D. & Kim, E. Y. Morphological alterations in the congenital blind based on the analysis of cortical thickness and surface area | Elsevier Enhanced Reader. (2009) doi:10.1016/j.neuroimage.2009.03.076.

13. Stroh, A.-L. *et al.* Blind individuals' enhanced ability to sense their own heartbeat is related to the thickness of their occipital cortex. *Cerebral Cortex* **34**, bhae324 (2024).

14. Hölig, C., Guerreiro, M. J. S., Lingareddy, S., Kekunnaya, R. & Röder, B. Sight restoration in congenitally blind humans does not restore visual brain structure. *Cerebral Cortex* bhac197 (2022) doi:10.1093/cercor/bhac197.

15. Fine, I. & Park, J.-M. Blindness and Human Brain Plasticity. *Annu. Rev. Vis. Sci.* **4**, 337–356 (2018).

16. Dzięgiel-Fivet, G. *et al.* Neural network for Braille reading and the speech-reading convergence in the blind: Similarities and differences to visual reading. *NeuroImage* **231**, 117851 (2021).

17. Kanjlia, S., Lane, C., Feigenson, L. & Bedny, M. Absence of visual experience modifies the neural basis of numerical thinking. *Proc Natl Acad Sci USA* **113**, 11172–11177 (2016).

18. Deen, B., Saxe, R. & Bedny, M. Occipital Cortex of Blind Individuals Is Functionally Coupled with Executive Control Areas of Frontal Cortex. *Journal of Cognitive Neuroscience* **27**, 1633–1647 (2015).

19. Bridge, H. & Watkins, K. E. Structural and functional brain reorganisation due to blindness: The special case of bilateral congenital anophthalmia. *Neuroscience & Biobehavioral Reviews* **107**, 765–774 (2019).

20. Markov, N. T. & Kennedy, H. The importance of being hierarchical. *Current Opinion in Neurobiology* **23**, 187–194 (2013).

21. Taylor, H. P. *et al.* Functional Hierarchy of the Human Neocortex from Cradle to Grave. Preprint at https://doi.org/10.1101/2024.06.14.599109 (2024).

22. Zhang, J. *et al.* Intrinsic Functional Connectivity is Organized as Three Interdependent Gradients. *Sci Rep* **9**, 15976 (2019).

23. Bethlehem, R. A. I. *et al.* Dispersion of functional gradients across the adult lifespan. *NeuroImage* **222**, 117299 (2020).

24. Friston, K. Functional integration and inference in the brain. *Progress in Neurobiology* **68**, 113–143

(2002).

25. Valk, S. L. *et al.* Functional and microstructural plasticity following social and interoceptive mental training. *eLife* **12**, e85188 (2023).
26. Haak, K. V., Marquand, A. F. & Beckmann, C. F. Connectopic mapping with resting-state fMRI. *NeuroImage* **170**, 83–94 (2018).
27. Watson, D. M. & Andrews, T. J. An evaluation of how connectopic mapping reveals visual field maps in V1. *Sci Rep* **12**, 16249 (2022).
28. Ngo, G. N., Haak, K. V., Beckmann, C. F. & Menon, R. S. Mesoscale hierarchical organization of primary somatosensory cortex captured by resting-state-fMRI in humans. *NeuroImage* **235**, 118031 (2021).
29. Song, Y. *et al.* Functional hierarchy of the angular gyrus and its underlying genetic architecture. *Human Brain Mapping* **44**, 2815–2828 (2023).
30. Tian, Y. & Zalesky, A. Characterizing the functional connectivity diversity of the insula cortex: Subregions, diversity curves and behavior. *NeuroImage* **183**, 716–733 (2018).
31. Wang, R. *et al.* Functional connectivity gradients of the insula to different cerebral systems. *Human Brain Mapping* **44**, 790–800 (2023).
32. Shen, Y. *et al.* Functional connectivity gradients of the cingulate cortex. *Commun Biol* **6**, 1–9 (2023).
33. Gordon, E. M. *et al.* Generation and Evaluation of a Cortical Area Parcellation from Resting-State Correlations. *Cereb. Cortex* **26**, 288–303 (2016).
34. Wig, G. S., Laumann, T. O. & Petersen, S. E. An approach for parcellating human cortical areas using resting-state correlations. *NeuroImage* **93**, 276–291 (2014).
35. Baum, G. L. *et al.* Development of structure–function coupling in human brain networks during youth. *Proc Natl Acad Sci USA* **117**, 771–778 (2020).
36. Paquola, C. *et al.* Microstructural and functional gradients are increasingly dissociated in transmodal

cortices. *PLOS Biology* **17**, e3000284 (2019).

37. Preti, M. G. & Van De Ville, D. Decoupling of brain function from structure reveals regional behavioral specialization in humans. *Nat Commun* **10**, 4747 (2019).
38. Vázquez-Rodríguez, B. *et al.* Gradients of structure–function tethering across neocortex. *Proceedings of the National Academy of Sciences* **116**, 21219–21227 (2019).
39. Pelland, M. *et al.* State-dependent modulation of functional connectivity in early blind individuals. *NeuroImage* **147**, 532–541 (2017).
40. Gorgolewski, K. J. *et al.* The brain imaging data structure, a format for organizing and describing outputs of neuroimaging experiments. *Sci Data* **3**, 160044 (2016).
41. Bedny, M. & Tian, M. Blindness Resting State. ICPSR - Interuniversity Consortium for Political and Social Research https://doi.org/10.3886/E198832V1 (2024).
42. Tian, M., Xiao, X., Hu, H., Cusack, R. & Bedny, M. Visual experience shapes functional connectivity between occipital and non-visual networks. *eLife* **13**, (2024).
43. Cruces, R. R. *et al.* Micapipe: A pipeline for multimodal neuroimaging and connectome analysis. *NeuroImage* **263**, 119612 (2022).
44. Cox, R. W. AFNI: software for analysis and visualization of functional magnetic resonance neuroimages. *Comput Biomed Res* **29**, 162–173 (1996).
45. Jenkinson, M., Beckmann, C. F., Behrens, T. E. J., Woolrich, M. W. & Smith, S. M. FSL. *Neuroimage* **62**, 782–790 (2012).
46. Avants, B. B., Epstein, C. L., Grossman, M. & Gee, J. C. Symmetric diffeomorphic image registration with cross-correlation: Evaluating automated labeling of elderly and neurodegenerative brain. *Medical Image Analysis* **12**, 26–41 (2008).
47. Dale, A. M., Fischl, B. & Sereno, M. I. Cortical Surface-Based Analysis: I. Segmentation and Surface Reconstruction. *NeuroImage* **9**, 179–194 (1999).

48. Henschel, L. *et al.* FastSurfer - A fast and accurate deep learning based neuroimaging pipeline. *NeuroImage* **219**, 117012 (2020).

49. Glasser, M. F. *et al.* A multi-modal parcellation of human cerebral cortex. *Nature* **536**, 171–178 (2016).

50. Satterthwaite, T. D. *et al.* An improved framework for confound regression and filtering for control of motion artifact in the preprocessing of resting-state functional connectivity data. *Neuroimage* **64**, 240–256 (2013).

51. Vos de Wael, R. *et al.* BrainSpace: a toolbox for the analysis of macroscale gradients in neuroimaging and connectomics datasets. *Commun Biol* **3**, 1–10 (2020).

52. Worsley, K. *et al.* SurfStat: A Matlab toolbox for the statistical analysis of univariate and multivariate surface and volumetric data using linear mixed effects models and random field theory. *NeuroImage* **47**, S102 (2009).

53. Yeo, B. T. T. *et al.* The organization of the human cerebral cortex estimated by intrinsic functional connectivity. *Journal of Neurophysiology* **106**, 1125–1165 (2011).

54. Posit team. Rstudio: Integrated. Posit Software, PBC (2024).

55. Singmann, H., Bolker, B., Westfall, J., Aust, F. & Ben-Shachar, M. S. _afex: Analysis of Factorial Experiments_. (2023).

56. Lenth, R. V. _emmeans: Estimated Marginal Means, aka Least-Squares Means_. (2023).

57. Fortin, J.-P. *et al.* Harmonization of multi-site diffusion tensor imaging data. *NeuroImage* **161**, 149–170 (2017).

58. Fortin, J.-P. *et al.* Harmonization of cortical thickness measurements across scanners and sites. *Neuroimage* **167**, 104–120 (2018).

59. Johnson, W. E., Li, C. & Rabinovic, A. Adjusting batch effects in microarray expression data using empirical Bayes methods. *Biostatistics* **8**, 118–127 (2007).

60. Paquola, C. *et al.* The architecture of the human default mode network explored through cytoarchitecture, wiring and signal flow. *Nat Neurosci* 1–11 (2025) doi:10.1038/s41593-024-01868-0.

61. Kim, J. S., Kanjlia, S., Merabet, L. B. & Bedny, M. Development of the Visual Word Form Area Requires Visual Experience: Evidence from Blind Braille Readers. *J. Neurosci.* **37**, 11495–11504 (2017).

62. Lane, C., Kanjlia, S., Omaki, A. & Bedny, M. 'Visual' Cortex of Congenitally Blind Adults Responds to Syntactic Movement. *Journal of Neuroscience* **35**, 12859–12868 (2015).

63. Bedny, M. Evidence from Blindness for a Cognitively Pluripotent Cortex. *Trends in Cognitive Sciences* **21**, 637–648 (2017).

64. Smallwood, J. *et al.* The default mode network in cognition: a topographical perspective. *Nat Rev Neurosci* **22**, 503–513 (2021).

65. Dixon, M. L. *et al.* Heterogeneity within the frontoparietal control network and its relationship to the default and dorsal attention networks. *Proceedings of the National Academy of Sciences* **115**, E1598–E1607 (2018).

66. Marek, S. & Dosenbach, N. U. F. The frontoparietal network: function, electrophysiology, and importance of individual precision mapping. *Dialogues in Clinical Neuroscience* **20**, 133–140 (2018).

67. Cole, M. W. *et al.* Multi-task connectivity reveals flexible hubs for adaptive task control. *Nat Neurosci* **16**, 1348–1355 (2013).

68. Collignon, O. *et al.* Functional specialization for auditory-spatial processing in the occipital cortex of congenitally blind humans. *Proceedings of the National Academy of Sciences* **108**, 4435–4440 (2011).

69. Qin, W., Liu, Y., Jiang, T. & Yu, C. The Development of Visual Areas Depends Differently on Visual Experience. *PLoS ONE* **8**, e53784 (2013).

70. Pietrini, P. *et al.* Beyond sensory images: Object-based representation in the human ventral pathway.

Proc Natl Acad Sci U S A **101**, 5658–5663 (2004).

71. Dormal, G., Rezk, M., Yakobov, E., Lepore, F. & Collignon, O. Auditory motion in the sighted and blind: Early visual deprivation triggers a large-scale imbalance between auditory and “visual” brain regions. *NeuroImage* **134**, 630–644 (2016).
72. Saadon-Grosman, N., Arzy, S. & Loewenstein, Y. Hierarchical cortical gradients in somatosensory processing. *NeuroImage* **222**, 117257 (2020).
73. Sen, S. *et al.* The Role of Visual Experience in Individual Differences of Brain Connectivity. *J. Neurosci.* **42**, 5070–5084 (2022).
74. Rakic, P., Suner, I. & Williams, R. W. A novel cytoarchitectonic area induced experimentally within the primate visual cortex. *Proceedings of the National Academy of Sciences* **88**, 2083–2087 (1991).
75. Magrou, L. *et al.* How Areal Specification Shapes the Local and Interareal Circuits in a Macaque Model of Congenital Blindness. *Cerebral Cortex* **28**, 3017–3034 (2018).
76. Hong, Y. *et al.* Structural and functional connectome relationships in early childhood. *Developmental Cognitive Neuroscience* **64**, 101314 (2023).
77. Natu, V. S. *et al.* Infants’ cortex undergoes microstructural growth coupled with myelination during development. *Commun Biol* **4**, 1191 (2021).
78. Fotiadis, P. *et al.* Myelination and excitation-inhibition balance synergistically shape structure-function coupling across the human cortex. *Nat Commun* **14**, 6115 (2023).
79. Natu, V. S. *et al.* Apparent thinning of human visual cortex during childhood is associated with myelination. *Proc Natl Acad Sci USA* **116**, 20750–20759 (2019).
80. Coullon, G. S. L., Emir, U. E., Fine, I., Watkins, K. E. & Bridge, H. Neurochemical changes in the pericalcarine cortex in congenital blindness attributable to bilateral anophthalmia. *J Neurophysiol* **114**, 1725–1733 (2015).
81. Rączy, K. *et al. Typical Resting State Activity of the Brain Requires Visual Input during an Early*

Sensitive Period. http://biorxiv.org/lookup/doi/10.1101/2021.06.09.446724 (2021) doi:10.1101/2021.06.09.446724.

82. Suárez, L. E., Markello, R. D., Betzel, R. F. & Misic, B. Linking Structure and Function in Macroscale Brain Networks. *Trends in Cognitive Sciences* **24**, 302–315 (2020).
83. Tu, J. C. *et al.* Early Life Neuroimaging: The Generalizability of Cortical Area Parcellations Across Development. Preprint at https://doi.org/10.1101/2024.09.09.612056 (2024).
84. Fotiadis, P. *et al.* Structure–function coupling in macroscale human brain networks. *Nat. Rev. Neurosci.* **25**, 688–704 (2024).
85. Benson, N. C. *et al.* The Retinotopic Organization of Striate Cortex Is Well Predicted by Surface Topology. *Current Biology* **22**, 2081–2085 (2012).
86. Natu, V. S. *et al.* Sulcal Depth in the Medial Ventral Temporal Cortex Predicts the Location of a Place-Selective Region in Macaques, Children, and Adults. *Cerebral Cortex* **31**, 48–61 (2021).
87. Weiner, K. S. & Grill-Spector, K. Sparsely-distributed organization of face and limb activations in human ventral temporal cortex. *NeuroImage* **52**, 1559–1573 (2010).

Supplementary Materials

Supplementary tables can be found at: [Supplementary Tables]

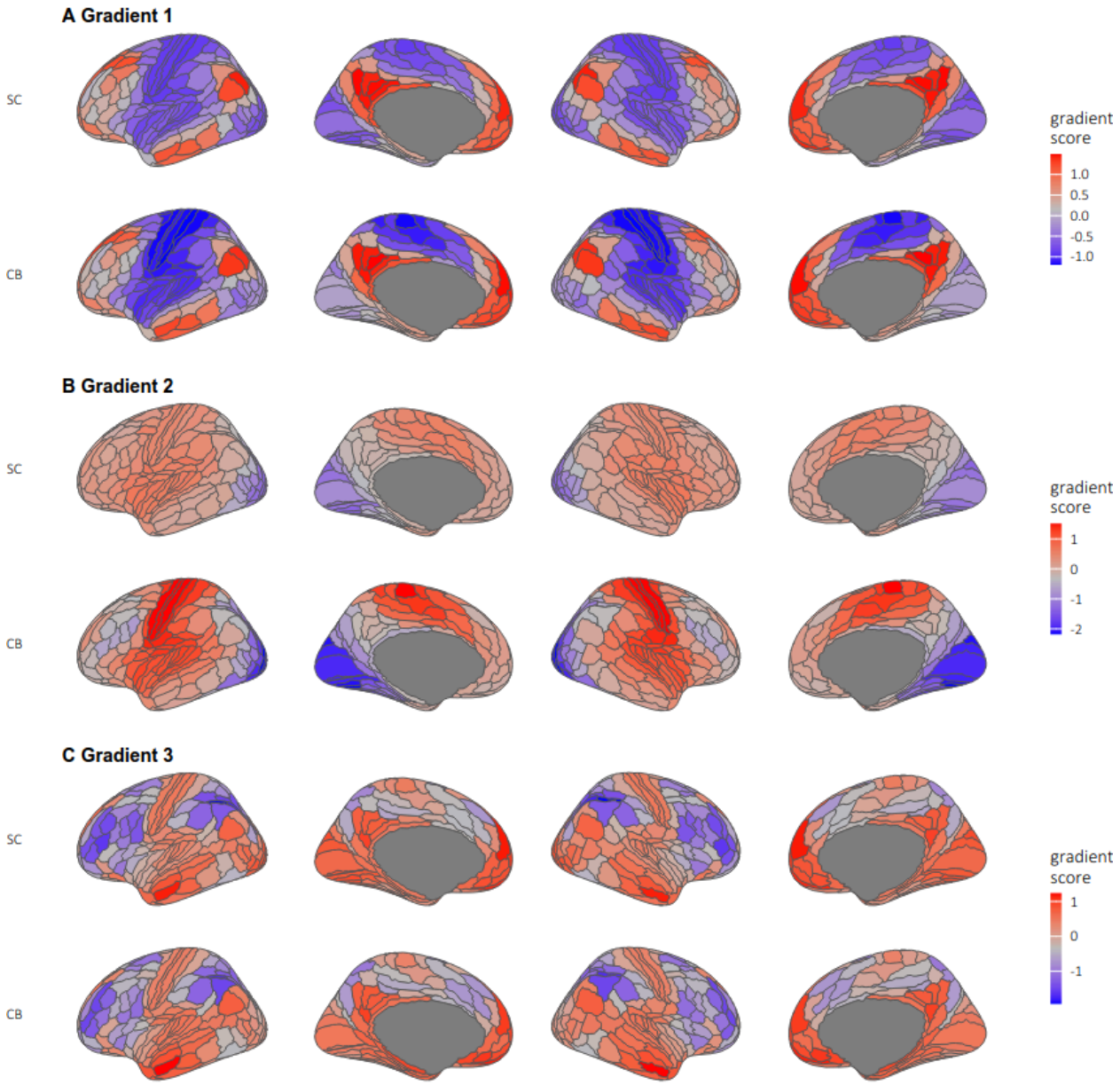

Supplementary Figure 1: First three mean gradients in sighted and blind groups. SC: Sighted Control Group, CB: Congenitally Blind Group

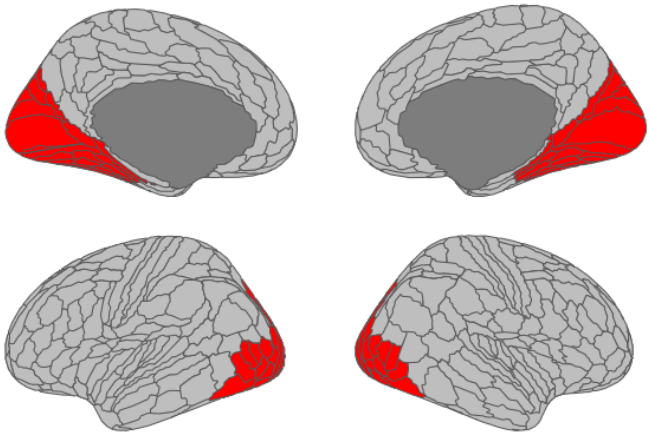

Supplementary Figure 2 | Network mask that is used to calculate connectivity gradients within visual areas.

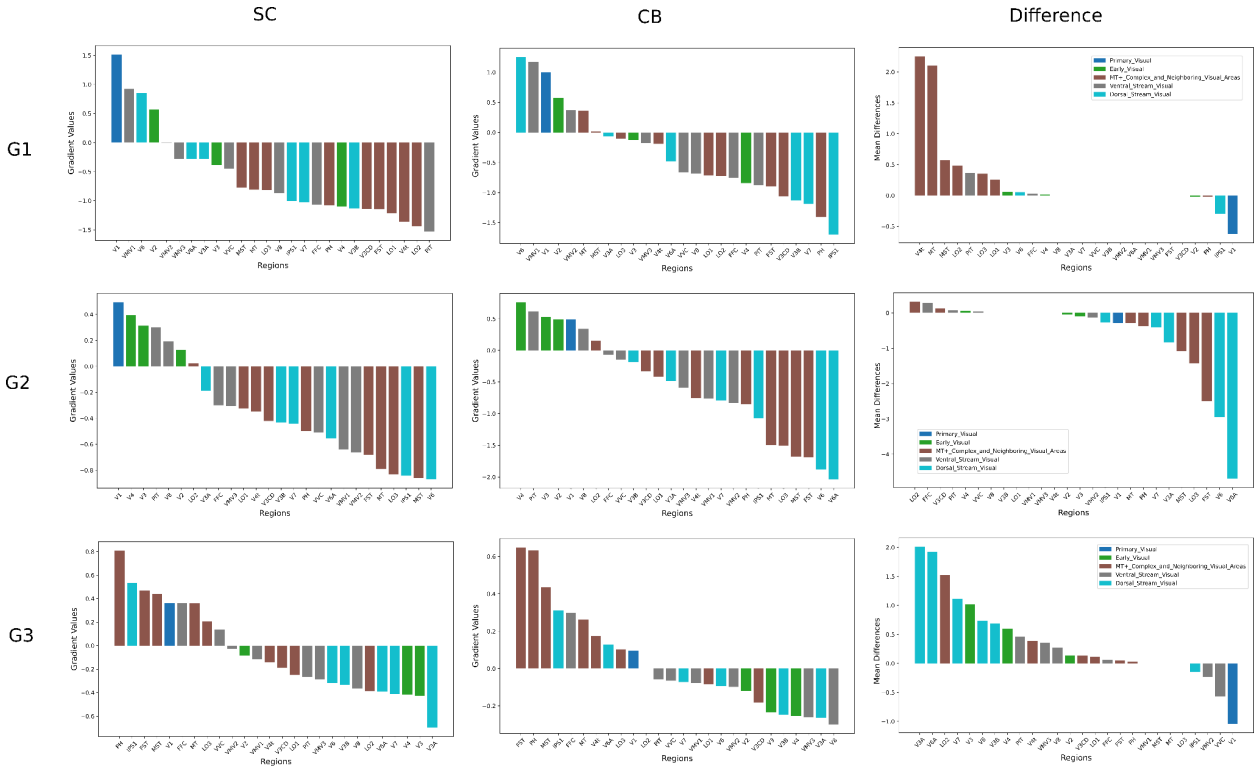

Supplementary Figure 3 | Decomposition of the vertex-wise gradients and their differences across visual regions. Left column: Mean gradients values across regions for sighted group. Mid panel: Mean gradients values across regions for blind group. Right column: Mean t-score of differences across regions (blind-sighted). SC: Sighted Control Group, CB: Congenitally Blind Group

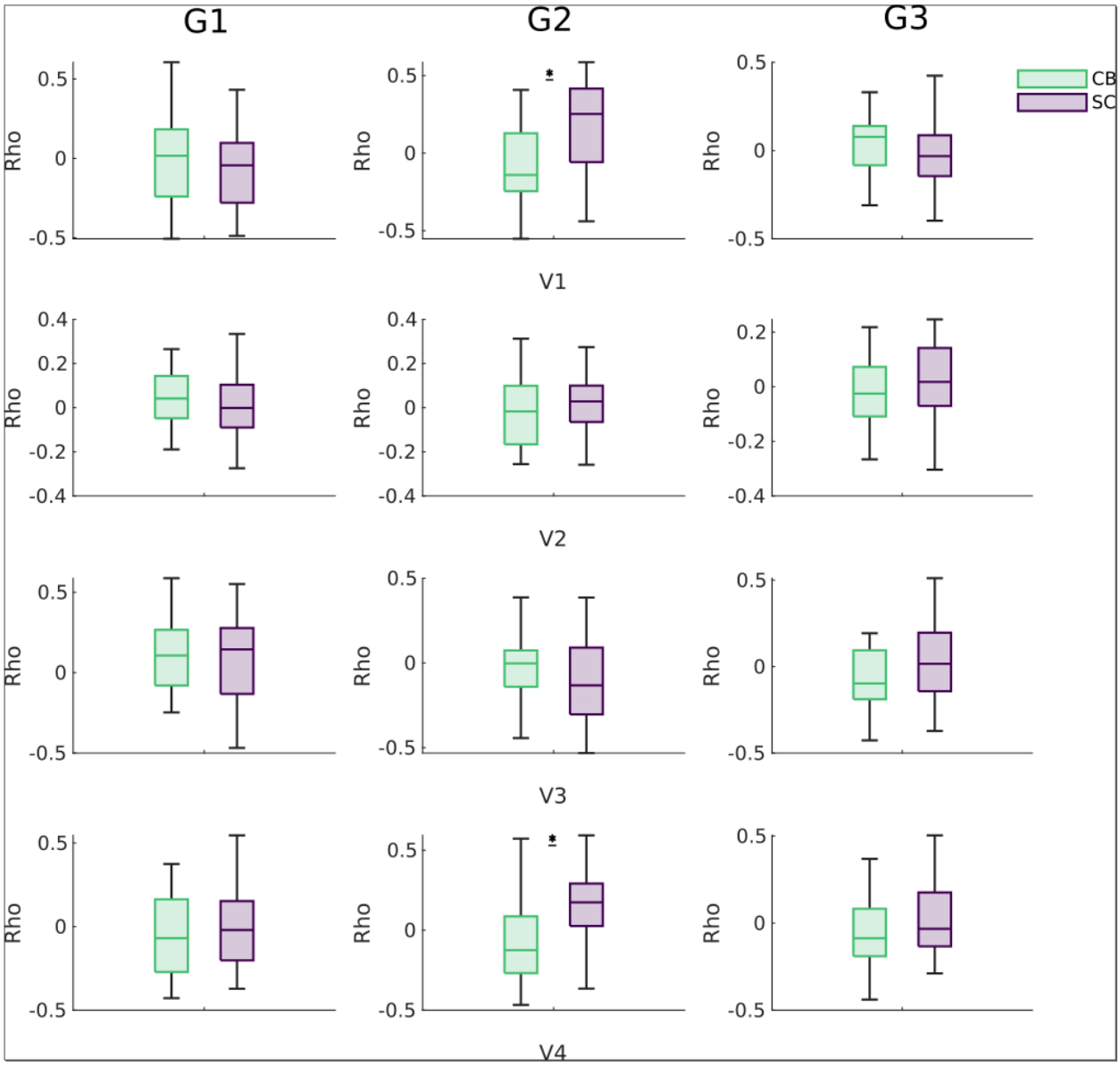

Supplementary Figure 4 | Structure-function coupling within visual areas across gradients. Asterisk indicates significant difference ($p<0.05$, corrected with FDR). SC: Sighted Control Group, CB: Congenitally Blind Group

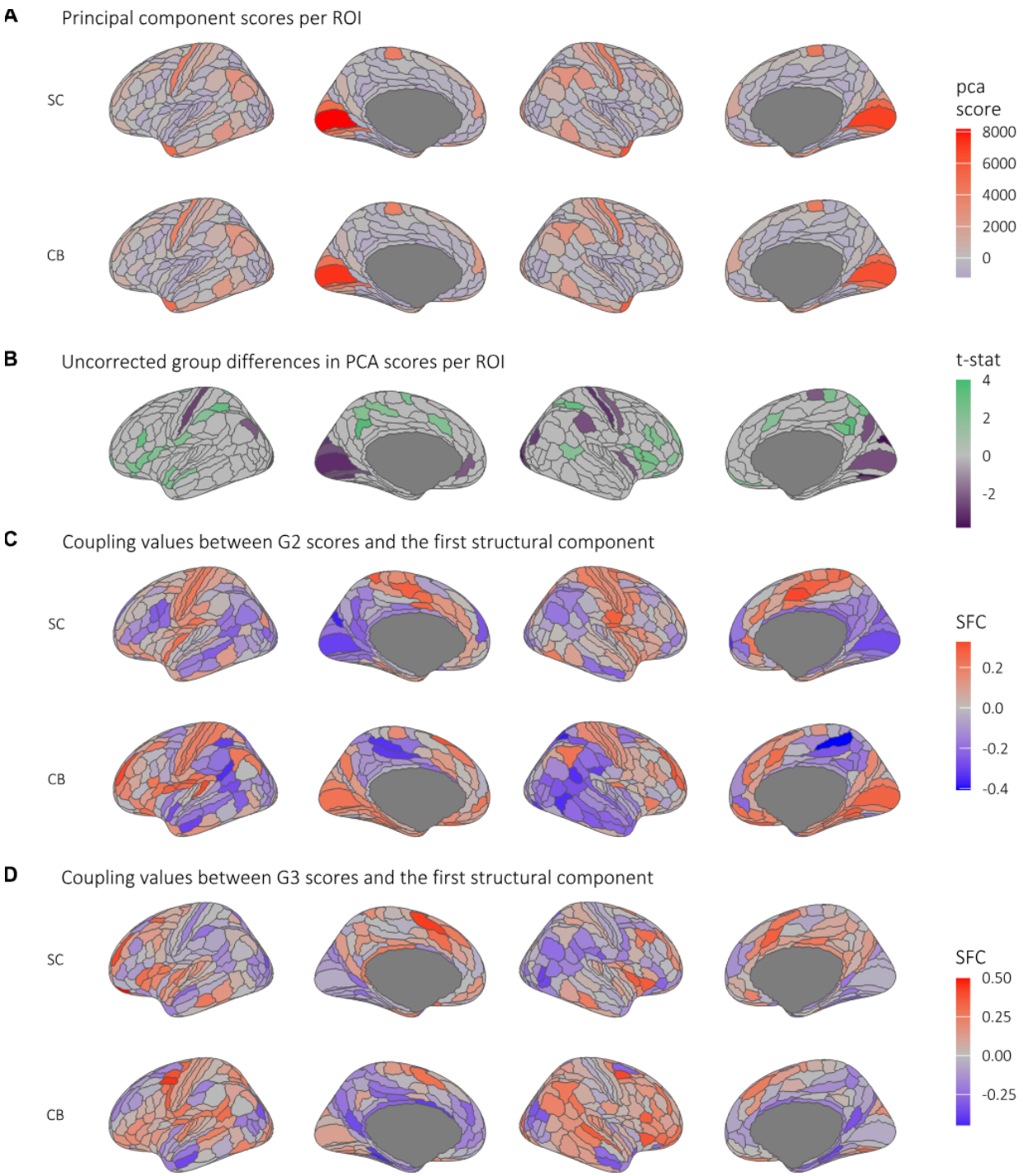

Supplementary Figure 5 | A Principal structural component for sighted and blind groups. **B** Uncorrected difference map of the structural component (blind>sighted). The group of blind individuals showed lower component scores in visual and sensorimotor areas, and higher scores in higher-order areas ($p < 0.05$) **C-D** Coupling values between the gradient scores of G2 and G3 and the first structural component. SC: Sighted Control Group, CB: Congenitally Blind Group

Table S1 - Regions that show significant differences gradient 1 scores between CB-SC groups.

region	hemi	yeo	stream	estimate	parameter	statistic	p (uncorr)	p (corr)
V3A	left	VIS	dorsal	0.447	80.351	3.660	< 0.001	0.006
V3A	right	VIS	dorsal	0.537	79.675	4.314	< 0.001	0.001
V3B	left	VIS	dorsal	0.656	78.468	4.841	< 0.001	< 0.001
V3B	right	VIS	dorsal	0.577	79.093	4.283	< 0.001	0.001
V7	left	VIS	dorsal	0.430	81.819	3.490	0.001	0.009
V1	left	VIS	evc	0.416	81.057	3.241	0.002	0.018
V1	right	VIS	evc	0.408	82.986	2.859	0.005	0.039
V2	left	VIS	evc	0.721	78.664	5.523	< 0.001	< 0.001
V2	right	VIS	evc	0.638	80.736	4.487	< 0.001	0.001
V3	left	VIS	evc	0.621	82.925	5.348	< 0.001	< 0.001
V3	right	VIS	evc	0.627	82.602	5.166	< 0.001	< 0.001
V4	left	VIS	evc	0.669	82.738	5.439	< 0.001	< 0.001
V4	right	VIS	evc	0.645	82.446	5.071	< 0.001	< 0.001
LO1	left	VIS	lateral	0.514	82.200	3.883	< 0.001	0.003
LO1	right	VIS	lateral	0.489	81.603	3.642	< 0.001	0.006
LO2	left	VIS	lateral	0.547	82.065	4.682	< 0.001	< 0.001
LO2	right	VIS	lateral	0.62	82.489	4.809	< 0.001	< 0.001
V3CD	left	VIS	lateral	0.621	81.492	4.450	< 0.001	0.001
V3CD	right	VIS	lateral	0.537	82.916	3.701	< 0.001	0.005
V4t	left	VIS	lateral	0.400	82.245	3.144	0.002	0.022
V4t	right	VIS	lateral	0.422	79.910	2.995	0.004	0.032
FFC	left	VIS	ventral	0.580	81.860	4.406	< 0.001	0.001
FFC	right	VIS	ventral	0.470	82.424	3.933	< 0.001	0.003
PIT	left	VIS	ventral	0.623	82.700	5.150	< 0.001	< 0.001
PIT	right	VIS	ventral	0.633	82.754	5.095	< 0.001	< 0.001
V8	left	VIS	ventral	0.607	82.845	5.021	< 0.001	< 0.001
V8	right	VIS	ventral	0.581	81.759	4.479	< 0.001	0.001
VMV1	left	VIS	ventral	0.702	77.719	5.175	< 0.001	< 0.001
VMV1	right	VIS	ventral	0.832	77.323	5.448	< 0.001	< 0.001
VMV2	right	VIS	ventral	0.391	82.950	2.879	0.005	0.038
VMV3	left	VIS	ventral	0.438	82.881	3.100	0.003	0.024
VMV3	right	VIS	ventral	0.506	82.992	3.836	< 0.001	0.003
VVC	left	VIS	ventral	0.510	82.954	3.951	< 0.001	0.003
VVC	right	VIS	ventral	0.444	81.540	3.221	0.002	0.018
24dd	left	SMN		-0.348	74.050	-2.959	0.004	0.032
24dv	left	SMN		-0.354	70.800	-2.976	0.004	0.032
5L	left	SMN		-0.337	80.121	-3.129	0.002	0.023
5m	right	SMN		-0.344	82.984	-2.895	0.005	0.037
7AL	left	DAN		-0.306	73.966	-3.261	0.002	0.018
7AL	right	DAN		-0.384	78.703	-3.850	< 0.001	0.003
7Am	left	DAN		-0.513	77.260	-4.109	< 0.001	0.002
7PC	left	DAN		-0.387	77.159	-3.837	< 0.001	0.004

7PL	left	DAN	-0.423	77.239	-3.455	0.001	0.010
AIP	left	DAN	-0.386	82.445	-3.630	< 0.001	0.006
AIP	right	DAN	-0.387	81.846	-3.189	0.002	0.020
PFt	right	DAN	-0.345	78.839	-2.992	0.004	0.032
6r	right	VAN	-0.336	80.030	-2.843	0.006	0.041
FOP3	right	VAN	-0.371	72.567	-2.963	0.004	0.032
PeEc	right	LIN	0.521	70.915	3.823	< 0.001	0.004
TGv	left	LIN	0.478	74.969	2.970	0.004	0.032

Table S2 Regions that show significant differences gradient 2 scores between CB-SC groups

region	hemi	yeo	stream	estimate	parameter	statistic	p (uncorr)	p (corr)
V3B	left	VIS	dorsal	-0.563	60.914	-2.526	0.014	0.027
V3B	right	VIS	dorsal	-0.597	59.309	-2.527	0.014	0.027
V6A	left	VIS	dorsal	0.653	63.222	3.193	0.002	0.006
V6A	right	VIS	dorsal	0.587	65.686	2.809	0.007	0.014
V1	left	VIS	evc	-1.045	61.54	-4.683	< 0.001	< 0.001
V1	right	VIS	evc	-1.047	61.619	-4.905	< 0.001	< 0.001
V2	left	VIS	evc	-0.758	63.064	-3.394	0.001	0.003
V2	right	VIS	evc	-0.9	61.556	-4.251	< 0.001	< 0.001
V3	left	VIS	evc	-0.741	63.733	-3.42	0.001	0.003
V3	right	VIS	evc	-0.838	66.378	-3.796	< 0.001	0.001
V4	left	VIS	evc	-0.798	66.127	-3.799	< 0.001	0.001
V4	right	VIS	evc	-0.853	67.231	-4.028	< 0.001	0.001
LO1	right	VIS	lateral	-0.567	58.346	-2.356	0.022	0.04
LO2	left	VIS	lateral	-0.617	61.111	-2.605	0.012	0.023
LO2	right	VIS	lateral	-0.832	59.752	-3.901	< 0.001	0.001
V3CD	right	VIS	lateral	-0.79	67.112	-3.829	< 0.001	0.001
FFC	left	VIS	ventral	-0.951	62.885	-4.405	< 0.001	< 0.001
FFC	right	VIS	ventral	-1.138	65.146	-5.199	< 0.001	< 0.001
PIT	left	VIS	ventral	-0.814	62.607	-3.66	0.001	0.002
PIT	right	VIS	ventral	-0.934	62.209	-4.126	< 0.001	0.001
V8	left	VIS	ventral	-0.803	65.507	-3.495	0.001	0.003
V8	right	VIS	ventral	-0.825	62.302	-3.556	0.001	0.002
VMV1	left	VIS	ventral	-0.784	60.69	-3.351	0.001	0.004
VMV1	right	VIS	ventral	-0.765	58.344	-3.266	0.002	0.005
VMV2	left	VIS	ventral	-0.891	59.646	-3.846	< 0.001	0.001
VMV2	right	VIS	ventral	-0.833	60.159	-3.45	0.001	0.003
VMV3	left	VIS	ventral	-0.641	62.681	-2.616	0.011	0.022
VMV3	right	VIS	ventral	-0.885	68.304	-3.787	< 0.001	0.001
VVC	left	VIS	ventral	-1.001	68.263	-4.584	< 0.001	< 0.001
VVC	right	VIS	ventral	-0.970	68.826	-4.36	< 0.001	< 0.001
PHA1	left	VIS		-0.946	57.374	-4.771	< 0.001	< 0.001
PHA2	left	VIS		-0.770	64.362	-4.464	< 0.001	< 0.001
PHA3	left	VIS		-0.763	66.413	-4.107	< 0.001	0.001
PHA3	right	VIS		-0.708	57.817	-4.028	< 0.001	0.001
PreS	left	VIS		-0.761	57.66	-4.267	< 0.001	< 0.001
ProS	left	VIS		-0.681	57.717	-3.402	0.001	0.003
ProS	right	VIS		-0.56	53.269	-2.906	0.005	0.011
1	left	SMN		1.168	77.159	7.996	0	0
1	right	SMN		1.115	75.171	7.472	0	0
2	left	SMN		0.9	69.802	6.794	0	0
2	right	SMN		0.909	68.441	6.311	0	0
24dd	left	SMN		0.738	61.639	5.251	0	0
24dd	right	SMN		0.744	65.744	5.575	0	0

24dv	left	SMN	0.674	61.161	4.854	0	0
24dv	right	SMN	0.672	61.832	5.222	0	0
3a	left	SMN	1.014	74.412	7.076	0	0
3a	right	SMN	1.016	74.216	7.191	0	0
3b	left	SMN	1.013	73.802	7.305	0	0
3b	right	SMN	1.095	76.101	7.974	0	0
4	left	SMN	1.056	78.057	7.596	0	0
4	right	SMN	1.038	76.113	7.622	0	0
43	left	SMN	0.764	68.147	5.277	0	0
52	left	SMN	0.447	63.068	2.8	0.007	0.014
52	right	SMN	0.589	58.146	3.895	0	0.001
5L	left	SMN	0.911	72.204	6.283	0	0
5L	right	SMN	0.87	77.589	5.926	0	0
5m	left	SMN	0.894	69.895	5.806	0	0
5m	right	SMN	0.787	71.41	4.993	0	0
6d	left	SMN	0.929	73.468	6.529	0	0
6d	right	SMN	0.924	73.838	6.28	0	0
6mp	left	SMN	0.756	74.981	6.264	0	0
6mp	right	SMN	0.812	73.726	6	0	0
6v	left	SMN	0.72	61.05	5.139	0	0
6v	right	SMN	0.673	63.79	4.258	0	0
A1	left	SMN	0.578	62.484	3.589	0.001	0.002
A1	right	SMN	0.488	57.749	2.595	0.012	0.023
A4	left	SMN	0.596	63.439	3.836	0	0.001
A4	right	SMN	0.586	63.436	3.693	0	0.002
A5	left	SMN	0.594	75.143	3.893	0	0.001
A5	right	SMN	0.651	75.465	4.149	0	0
FOP2	left	SMN	0.661	59.786	4.243	0	0
Ig	left	SMN	0.789	64.489	4.996	0	0
Ig	right	SMN	0.684	60.508	4.076	0	0.001
LBelt	left	SMN	0.689	62.387	4.318	0	0
LBelt	right	SMN	0.638	61.824	3.832	0	0.001
MBelt	left	SMN	0.503	69.357	3.296	0.002	0.004
MBelt	right	SMN	0.481	63.364	2.977	0.004	0.009
OP1	left	SMN	0.817	63.416	5.503	0	0
OP1	right	SMN	0.835	68.158	5.514	0	0
OP2-3	left	SMN	0.848	68.625	5.165	0	0
OP2-3	right	SMN	0.622	58.698	3.567	0.001	0.002
OP4	left	SMN	0.818	68.702	5.676	0	0
OP4	right	SMN	0.862	64.453	5.438	0	0
PBelt	left	SMN	0.561	62.777	3.622	0.001	0.002
PBelt	right	SMN	0.559	64.622	3.52	0.001	0.002
PFcm	left	SMN	0.516	64.883	3.493	0.001	0.003
RI	left	SMN	0.789	66.34	4.956	0	0
RI	right	SMN	0.589	59.044	3.535	0.001	0.002
TA2	right	SMN	0.497	67.389	3.298	0.002	0.004

IPS1	left	DAN	dorsal	-0.708	59.708	-3.515	0.001	0.003
IPS1	right	DAN	dorsal	-0.635	61.996	-2.954	0.004	0.01
PH	left	DAN	lateral	-0.657	60.513	-3.098	0.003	0.007
PH	right	DAN	lateral	-0.772	52.987	-3.266	0.002	0.005
7AL	left	DAN		0.783	82.172	5.088	0	0
7AL	right	DAN		0.701	80.32	4.792	0	0
7Am	left	DAN		0.485	75.326	3.496	0.001	0.002
7PC	left	DAN		0.677	76.139	4.919	0	0
7PC	right	DAN		0.5	65.078	3.204	0.002	0.005
IFJp	left	DAN		-0.843	57.741	-5.196	0	0
IFJp	right	DAN		-0.995	55.906	-6.531	0	0
IP0	left	DAN		-0.88	65.684	-4.389	0	0
IP0	right	DAN		-1.144	55.336	-5.37	0	0
LIPd	left	DAN		-0.543	67.132	-3.288	0.002	0.004
LIPd	right	DAN		-0.598	67.068	-4.061	< 0.001	0.001
MIP	left	DAN		-0.557	69.137	-3.246	0.002	0.005
MIP	right	DAN		-0.544	62.568	-3.02	0.004	0.008
PEF	right	DAN		-0.711	56.518	-3.626	0.001	0.002
PFt	left	DAN		0.52	64.768	3.691	< 0.001	0.002
PFt	right	DAN		0.443	55.714	2.962	0.004	0.01
PGp	left	DAN		-0.71	67.148	-3.754	< 0.001	0.001
PGp	right	DAN		-0.889	57.931	-5.15	< 0.001	< 0.001
TE2p	right	DAN		-0.66	55.007	-3.468	0.001	0.003
VIP	left	DAN		0.635	81.658	3.558	0.001	0.002
VIP	right	DAN		0.372	76.121	2.649	0.01	0.02
23c	left	VAN		0.446	76.398	4.077	< 0.001	0.001
23c	right	VAN		0.545	70.956	4.244	< 0.001	< 0.001
43	right	VAN		0.808	64.255	5.423	< 0.001	< 0.001
5mv	left	VAN		0.644	71.008	5.582	< 0.001	< 0.001
5mv	right	VAN		0.642	70.208	5.086	< 0.001	< 0.001
AAIC	left	VAN		0.315	82.772	3.134	0.002	0.006
FOP1	left	VAN		0.578	65.926	4.104	< 0.001	0.001
FOP1	right	VAN		0.396	60.033	2.456	0.017	0.032
FOP3	left	VAN		0.501	64.292	3.349	0.001	0.004
FOP3	right	VAN		0.447	69.002	2.878	0.005	0.011
FOP4	left	VAN		0.366	66.75	2.99	0.004	0.009
FOP4	right	VAN		0.313	73.143	2.365	0.021	0.039
MI	left	VAN		0.328	71.844	2.915	0.005	0.01
MI	right	VAN		0.333	71.716	2.964	0.004	0.009
PFcm	right	VAN		0.51	61.527	3.32	0.002	0.004
PFop	left	VAN		0.486	64.331	3.95	< 0.001	0.001
PFop	right	VAN		0.588	58.928	4.479	< 0.001	< 0.001
PI	right	VAN		0.364	63.676	2.49	0.015	0.029
PSL	left	VAN		0.396	69.974	3.245	0.002	0.005
PoI1	left	VAN		0.46	62.015	3.144	0.003	0.006
PoI1	right	VAN		0.484	59.685	3.425	0.001	0.003

PoI2	left	VAN	0.534	59.267	3.877	< 0.001	0.001
PoI2	right	VAN	0.524	62.265	4.013	< 0.001	0.001
SCEF	left	VAN	0.529	64.93	4.419	< 0.001	< 0.001
SCEF	right	VAN	0.47	70.971	3.554	0.001	0.002
TPOJ1	left	VAN	0.458	73.865	2.759	0.007	0.015
a24pr	left	VAN	0.352	57.8	3.463	0.001	0.003
a24pr	right	VAN	0.343	65.527	2.983	0.004	0.009
p24pr	left	VAN	0.427	54.193	3.358	0.001	0.004
p24pr	right	VAN	0.505	57.851	4.512	< 0.001	< 0.001
p32pr	left	VAN	0.301	67.146	2.974	0.004	0.009
p32pr	right	VAN	0.32	63.51	2.454	0.017	0.032
Pir	right	LIN	0.361	78.951	2.768	0.007	0.015
TF	left	LIN	-0.339	56.076	-2.297	0.025	0.046
TF	right	LIN	-0.336	64.464	-2.67	0.01	0.019
TGd	right	LIN	0.263	74.822	2.339	0.022	0.04
11l	left	FPN	-0.279	64.679	-2.321	0.023	0.043
44	left	FPN	-0.391	52.578	-3.171	0.003	0.006
8BM	left	FPN	-0.309	60.417	-2.803	0.007	0.014
8BM	right	FPN	-0.279	55.026	-2.296	0.026	0.046
8C	left	FPN	-0.406	47.161	-3.126	0.003	0.007
8C	right	FPN	-0.441	49.938	-3.482	0.001	0.003
IFJa	left	FPN	-0.671	61.04	-4.066	< 0.001	0.001
IFJa	right	FPN	-0.817	49.949	-5.45	< 0.001	< 0.001
IFSa	left	FPN	-0.656	59.174	-4.882	< 0.001	< 0.001
IFSa	right	FPN	-0.73	56.52	-4.959	< 0.001	< 0.001
IFSp	left	FPN	-0.713	59.882	-4.808	< 0.001	< 0.001
IFSp	right	FPN	-0.829	47.012	-4.686	< 0.001	< 0.001
IP1	left	FPN	-0.822	52.574	-6.027	< 0.001	< 0.001
IP1	right	FPN	-1.036	52.404	-6.137	< 0.001	< 0.001
IP2	left	FPN	-0.523	69.085	-4.373	< 0.001	< 0.001
IP2	right	FPN	-0.543	64.515	-4.091	< 0.001	0.001
PFm	left	FPN	-0.418	59.825	-4.577	< 0.001	< 0.001
POS2	left	FPN	-0.435	66.16	-3.498	0.001	0.003
a47r	left	FPN	-0.318	52.386	-2.624	0.011	0.022
a9-46v	left	FPN	-0.391	61.286	-4.3	< 0.001	< 0.001
i6-8	left	FPN	-0.369	56.683	-2.987	0.004	0.009
i6-8	right	FPN	-0.358	61.855	-2.957	0.004	0.01
p47r	left	FPN	-0.439	70.404	-3.927	< 0.001	0.001
p47r	right	FPN	-0.489	63.531	-4.279	< 0.001	< 0.001
p9-46v	left	FPN	-0.608	53.404	-4.804	< 0.001	< 0.001
p9-46v	right	FPN	-0.342	53.791	-2.653	0.01	0.021
s6-8	left	FPN	-0.228	65.552	-2.346	0.022	0.04
44	right	DMN	-0.376	58.596	-3.088	0.003	0.007
PFm	right	DMN	-0.32	58.45	-2.989	0.004	0.009
PGs	left	DMN	-0.24	61.51	-2.754	0.008	0.016
PGs	right	DMN	-0.279	59.63	-2.934	0.005	0.01

PHA1	right	DMN	-0.671	56.312	-3.719	< 0.001	0.002
PHA2	right	DMN	-0.526	57.245	-3.187	0.002	0.006
POS1	left	DMN	-0.444	67.579	-3.319	0.001	0.004
POS1	right	DMN	-0.389	66.295	-3.019	0.004	0.008
POS2	right	DMN	-0.341	61.515	-2.732	0.008	0.017
PreS	right	DMN	-0.613	52.725	-3.953	< 0.001	0.001
RSC	left	DMN	-0.336	69.896	-2.786	0.007	0.014
STGa	right	DMN	0.499	66.973	4.12	< 0.001	0.001
STSda	right	DMN	0.424	72.594	3.082	0.003	0.007
STSdp	left	DMN	0.549	71.6	3.606	0.001	0.002
STSdp	right	DMN	0.431	71.202	3.091	0.003	0.007
STSva	right	DMN	0.331	68.213	3.237	0.002	0.005
STSvp	left	DMN	0.448	60.457	3.546	0.001	0.002
STSvp	right	DMN	0.5	64.673	4.16	< 0.001	< 0.001
TE1a	right	DMN	0.22	65.458	2.373	0.021	0.039
TE1m	right	DMN	0.254	71.436	2.6	0.011	0.022
a47r	right	DMN	-0.389	52.509	-3.111	0.003	0.007
s6-8	right	DMN	-0.241	64.881	-2.419	0.018	0.035

Table S3 Regions that show significant differences gradient 3 scores between CB-SC groups

region	hemi	yeo	stream	estimate	parameter	statistic	p (uncorr)	p (corr)
V3A	left	VIS	dorsal	-0.802	76.887	-6.8	< 0.001	<0.001
V3A	right	VIS	dorsal	-0.671	76.095	-5.456	< 0.001	<0.001
V3B	left	VIS	dorsal	-0.717	78.274	-4.086	< 0.001	0.002
V3B	right	VIS	dorsal	-0.707	82.891	-3.947	< 0.001	0.002
V6	left	VIS	dorsal	-0.461	82.382	-3.286	0.001	0.015
V6	right	VIS	dorsal	-0.382	82.917	-2.942	0.004	0.037
V6A	left	VIS	dorsal	-0.901	82.883	-5.918	< 0.001	<0.001
V6A	right	VIS	dorsal	-0.887	82.799	-6.388	< 0.001	<0.001
V7	left	VIS	dorsal	-0.849	82.036	-4.451	< 0.001	0.001
V7	right	VIS	dorsal	-0.75	82.994	-5.019	< 0.001	<0.001
V2	left	VIS	evc	-0.417	70.749	-3.538	0.001	0.009
V3	left	VIS	evc	-0.677	74.911	-5.386	< 0.001	<0.001
V3	right	VIS	evc	-0.615	80.007	-5.531	< 0.001	<0.001
V4	left	VIS	evc	-0.805	76.29	-6.222	< 0.001	<0.001
V4	right	VIS	evc	-0.809	77.34	-6.173	< 0.001	<0.001
LO1	left	VIS	lateral	-0.69	71.127	-4.164	< 0.001	0.001
LO2	left	VIS	lateral	-0.578	77.054	-5.054	< 0.001	<0.001
LO2	right	VIS	lateral	-0.563	82.16	-4.559	< 0.001	<0.001
V3CD	left	VIS	lateral	-0.591	82.224	-3.834	< 0.001	0.003
V4t	left	VIS	lateral	-0.415	82.54	-3.402	0.001	0.011
V4t	right	VIS	lateral	-0.407	82.888	-3.241	0.002	0.017
PIT	left	VIS	ventral	-0.686	75.162	-4.77	< 0.001	<0.001
PIT	right	VIS	ventral	-0.485	82.446	-3.727	< 0.001	0.005
V8	left	VIS	ventral	-0.654	81.328	-4.862	< 0.001	<0.001
V8	right	VIS	ventral	-0.582	80.01	-4.147	< 0.001	0.001
VMV3	right	VIS	ventral	-0.476	76.647	-3.204	0.002	0.019
DVT	left	VIS		-0.562	81.685	-3.024	0.003	0.03
PHA2	left	VIS		0.509	82.525	3.469	0.001	0.009
IFJp	right	DAN		0.658	82.945	3.369	0.001	0.012
IP0	right	DAN		0.665	81.71	3.13	0.002	0.023
PGp	right	DAN		0.766	82.741	4.5	< 0.001	<0.001
TE2p	right	DAN		0.901	82.618	4.538	< 0.001	<0.001
H	left	LIN		0.438	81.151	3.652	< 0.001	0.006
H	right	LIN		0.501	81.624	3.78	< 0.001	0.004
PeEc	right	LIN		0.712	76.749	4.623	< 0.001	<0.001
TF	left	LIN		0.71	77.996	4.682	< 0.001	<0.001
TF	right	LIN		0.655	80.531	3.968	< 0.001	0.002
IFJa	right	FPN		0.801	82.772	3.922	< 0.001	0.003
IFSa	right	FPN		0.58	82.478	3.028	0.003	0.03
IP1	right	FPN		0.855	80.633	4.479	< 0.001	<0.001
p24	right	DMN		-0.533	79.176	-3.477	0.001	0.009

Table S4 Summary of the regions that show significant differences in gradient scores between CB and SC groups across 3 gradients. For G1, G2, G3: If 1, then region shows a significant group difference.

region	hemi	stream	G1	G2	G3
V3A	left	dorsal	1	0	1
V3A	right	dorsal	1	0	1
V3B	left	dorsal	1	1	1
V3B	right	dorsal	1	1	1
V7	left	dorsal	1	0	1
V7	right	dorsal	0	0	1
V6A	left	dorsal	0	1	1
V6A	right	dorsal	0	1	1
V6	left	dorsal	0	0	1
V6	right	dorsal	0	0	1
V1	left	evc	1	1	0
V1	right	evc	1	1	0
V2	left	evc	1	1	1
V2	right	evc	1	1	0
V3	left	evc	1	1	1
V3	right	evc	1	1	1
V4	left	evc	1	1	1
V4	right	evc	1	1	1
LO1	left	lateral	1	0	1
LO1	right	lateral	1	1	0
LO2	left	lateral	1	1	1
LO2	right	lateral	1	1	1
V3CD	left	lateral	1	0	1
V3CD	right	lateral	1	1	0
V4t	left	lateral	1	0	1
V4t	right	lateral	1	0	1
FFC	left	ventral	1	1	0
FFC	right	ventral	1	1	0
PIT	left	ventral	1	1	1
PIT	right	ventral	1	1	1
V8	left	ventral	1	1	1
V8	right	ventral	1	1	1
VMV1	left	ventral	1	1	0
VMV1	right	ventral	1	1	0
VMV2	left	ventral	0	1	0
VMV2	right	ventral	1	1	0
VMV3	left	ventral	1	1	0
VMV3	right	ventral	1	1	1
VVC	left	ventral	1	1	0
VVC	right	ventral	1	1	0
PHA1	left	ventral	0	1	0

PHA2	left	ventral	0	1	1
PHA3	left	ventral	0	1	0
PHA3	right	ventral	0	1	0
PreS	left	ventral	0	1	0
ProS	left	ventral	0	1	0
ProS	right	ventral	0	1	0
DVT	left	ventral	0	0	1

Table S5 | Group differences in community-based profiles of the first three gradients.

yeo	gradient	estimate	parameter	statistic	p (uncorr)	CI (low)	CI (high)	p (corr)
VN	1	-0.392	51.925	-4.943	0	-0.551	-0.233	0
SMN	1	0.219	51.499	3.897	0	0.106	0.331	0.001
DAN	1	0.092	46.529	0.82	0.417	-0.134	0.317	0.486
VAN	1	0.2	51.116	2.693	0.01	0.051	0.35	0.022
LN	1	-0.175	27.903	-1.032	0.311	-0.523	0.172	0.435
FPN	1	0.104	53.84	1.128	0.264	-0.08	0.288	0.435
DMN	1	-0.044	97.997	-0.429	0.669	-0.249	0.161	0.669
VN	2	0.575	49.015	5.446	0	0.363	0.787	0
SMN	2	-0.7	42.367	-12.791	0	-0.811	-0.59	0
DAN	2	0.137	34.281	0.878	0.386	-0.18	0.453	0.386
VAN	2	-0.332	36.324	-4.889	0	-0.47	-0.194	0
LN	2	0.062	19.275	0.888	0.386	-0.083	0.206	0.386
FPN	2	0.318	39.347	4.759	0	0.183	0.453	0
DMN	2	0.058	69.038	0.972	0.334	-0.061	0.176	0.386
VN	3	0.304	52.754	3.999	0	0.152	0.457	0.001
SMN	3	-0.055	54.997	-0.971	0.336	-0.167	0.058	0.784
DAN	3	-0.109	47.652	-0.682	0.498	-0.431	0.213	0.787
VAN	3	-0.012	50.436	-0.112	0.911	-0.235	0.21	0.912
LN	3	-0.255	27.762	-2.153	0.04	-0.498	-0.012	0.141
FPN	3	-0.074	53.088	-0.584	0.562	-0.328	0.18	0.787
DMN	3	-0.011	98	-0.111	0.912	-0.212	0.19	0.912

Table S6 | Estimated marginal means of VN distance to the other 6 yeo networks in G1 per group and network. CB = congenitally blind, SC = sighted control.

group	yeo	emmean	SE	df	lower.CL	upper.CL
SC	SMN	0.319	0.083	281.246	0.155	0.483
CB	SMN	0.975	0.086	282.011	0.805	1.145
SC	DAN	0.333	0.083	281.246	0.169	0.497
CB	DAN	0.344	0.086	282.011	0.174	0.514
SC	VAN	0.294	0.083	281.246	0.129	0.458
CB	VAN	0.702	0.086	282.011	0.532	0.872
SC	LN	0.963	0.083	281.246	0.798	1.127
CB	LN	0.764	0.086	282.011	0.594	0.934
SC	FPN	1.003	0.083	281.246	0.839	1.167
CB	FPN	0.54	0.086	282.011	0.37	0.710
SC	DMN	1.295	0.083	281.246	1.13	1.459
CB	DMN	0.944	0.086	282.011	0.774	1.114

Table S7 | Results of post hoc tests assessing the effect of group on distance of VN to the other 6 yeo networks for each network in G1.

yeo	estimate	SE	df	t-ratio	p-value
SMN	**-0.656**	**0.12**	**281.43**	**-5.464**	**< 0.001**
DAN	-0.011	0.12	281.43	-0.094	0.925
VAN	**-0.408**	**0.12**	**281.43**	**-3.399**	**0.001**
LN	0.199	0.12	281.43	1.657	0.099
FPN	**0.463**	**0.12**	**281.43**	**3.858**	**< 0.001**
DMN	**0.351**	**0.12**	**281.43**	**2.92**	**0.004**

Table S8 | Estimated marginal means of VN distance to the other 6 yeo networks in G2 per group and network. CB = congenitally blind, SC = sighted control.

group	yeo	emmean	SE	df	lower.CL	upper.CL
SC	SMN	1.409	0.142	100.574	1.127	1.692
CB	SMN	2.679	0.147	100.657	2.386	2.971
SC	DAN	0.783	0.142	100.574	0.501	1.066
CB	DAN	1.215	0.147	100.657	0.923	1.508
SC	VAN	1.384	0.142	100.574	1.101	1.667
CB	VAN	2.285	0.147	100.657	1.993	2.577
SC	LN	1	0.142	100.574	0.717	1.283
CB	LN	1.506	0.147	100.657	1.214	1.798
SC	FPN	1.004	0.142	100.574	0.722	1.287
CB	FPN	1.255	0.147	100.657	0.963	1.548
SC	DMN	0.937	0.142	100.574	0.655	1.220
CB	DMN	1.449	0.147	100.657	1.156	1.741

Table 9 | Results of post hoc tests assessing the effect of group on distance of VN to the other 6 yeo networks for each network in G2.

yeo	estimate	SE	df	t-ratio	p-value
SMN	**-1.269**	**0.205**	**100.594**	**-6.190**	**< 0.001**
DAN	**-0.432**	**0.205**	**100.594**	**-2.108**	**0.038**
VAN	**-0.901**	**0.205**	**100.594**	**-4.394**	**< 0.001**
LN	**-0.506**	**0.205**	**100.594**	**-2.468**	**0.015**
FPN	-0.251	0.205	100.594	-1.225	0.224
DMN	**-0.511**	**0.205**	**100.594**	**-2.494**	**0.014**

Table S10 | Estimated marginal means of VN distance to the other 6 yeo networks in G3 per group and network. CB = congenitally blind, SC = sighted control.

group	yeo	emmean	SE	df	lower.CL	upper.CL
SC	SMN	0.333	0.057	341.77	0.220	0.446
CB	SMN	0.263	0.059	342.611	0.146	0.379
SC	DAN	1.185	0.057	341.77	1.072	1.297
CB	DAN	0.773	0.059	342.611	0.656	0.890
SC	VAN	0.873	0.057	341.77	0.761	0.986
CB	VAN	0.609	0.059	342.611	0.493	0.726
SC	LN	0.263	0.057	341.77	0.150	0.376
CB	LN	0.454	0.059	342.611	0.338	0.571
SC	FPN	1.442	0.057	341.77	1.329	1.555
CB	FPN	1.065	0.059	342.611	0.948	1.181
SC	DMN	0.28	0.057	341.77	0.167	0.393
CB	DMN	0.271	0.059	342.611	0.154	0.387

Table S11| Results of post hoc tests assessing the effect of group on distance of VN to the other 6 yeo networks for each network in G3.

yeo	estimate	SE	df	t-ratio	p-value
SMN	0.07	0.082	341.972	0.852	0.395
DAN	**0.412**	**0.082**	**341.972**	**4.993**	**< 0.001**
VAN	**0.264**	**0.082**	**341.972**	**3.202**	**0.001**
LN	**-0.191**	**0.082**	**341.972**	**-2.32**	**0.021**
FPN	**0.377**	**0.082**	**341.972**	**4.575**	**< 0.001**
DMN	0.009	0.082	341.972	0.113	0.910

Table S12| Occurence of the rank orders across 10000 bootstraps and 3 gradients

G1				G2				G3			
SC		CB		SC		CB		SC		CB	
rank combination	frequency	rank combination	frequency	rank combination	frequency	rank combination	frequency	rank combination	frequency	rank combination	frequency
V1-V2-V3-V4	4265	V1-V2-V3-V4	514	V1-V2-V3-V4	6147	V1-V2-V3-V4	5540	V1-V2-V3-V4	52	V1-V2-V3-V4	1506
V1-V2-V4-V3	2840	V1-V2-V4-V3	1213	V1-V2-V4-V3	3400	V1-V2-V4-V3	409	V1-V2-V4-V3	7	V1-V2-V4-V3	104
V1-V3-V2-V4	58	V1-V3-V2-V4	0	V1-V3-V2-V4	85	V1-V3-V2-V4	198	V1-V3-V2-V4	31	V1-V3-V2-V4	16
V1-V3-V4-V2	197	V1-V3-V4-V2	86	V1-V3-V4-V2	228	V1-V3-V4-V2	106	V1-V3-V4-V2	2	V1-V3-V4-V2	0
V1-V4-V2-V3	7	V1-V4-V2-V3	0	V1-V4-V2-V3	16	V1-V4-V2-V3	184	V1-V4-V2-V3	5	V1-V4-V2-V3	0
V1-V4-V3-V2	164	V1-V4-V3-V2	2	V1-V4-V3-V2	87	V1-V4-V3-V2	229	V1-V4-V3-V2	4	V1-V4-V3-V2	0
V2-V1-V3-V4	1954	V2-V1-V3-V4	863	V2-V1-V3-V4	35	V2-V1-V3-V4	1654	V2-V1-V3-V4	161	V2-V1-V3-V4	6942
V2-V1-V4-V3	234	V2-V1-V4-V3	2913	V2-V1-V4-V3	1	V2-V1-V4-V3	387	V2-V1-V4-V3	15	V2-V1-V4-V3	613
V2-V3-V1-V4	7	V2-V3-V1-V4	0	V2-V3-V1-V4	0	V2-V3-V1-V4	33	V2-V3-V1-V4	104	V2-V3-V1-V4	2
V2-V3-V4-V1	4	V2-V3-V4-V1	192	V2-V3-V4-V1	0	V2-V3-V4-V1	16	V2-V3-V4-V1	7	V2-V3-V4-V1	0
V2-V4-V1-V3	1	V2-V4-V1-V3	0	V2-V4-V1-V3	0	V2-V4-V1-V3	57	V2-V4-V1-V3	49	V2-V4-V1-V3	0
V2-V4-V3-V1	1	V2-V4-V3-V1	4	V2-V4-V3-V1	0	V2-V4-V3-V1	22	V2-V4-V3-V1	4	V2-V4-V3-V1	0
V3-V1-V2-V4	215	V3-V1-V2-V4	117	V3-V1-V2-V4	0	V3-V1-V2-V4	297	V3-V1-V2-V4	1242	V3-V1-V2-V4	568
V3-V1-V4-V2	8	V3-V1-V4-V2	2540	V3-V1-V4-V2	0	V3-V1-V4-V2	111	V3-V1-V4-V2	14	V3-V1-V4-V2	2
V3-V2-V1-V4	14	V3-V2-V1-V4	0	V3-V2-V1-V4	0	V3-V2-V1-V4	241	V3-V2-V1-V4	932	V3-V2-V1-V4	195
V3-V2-V4-V1	7	V3-V2-V4-V1	654	V3-V2-V4-V1	0	V3-V2-V4-V1	99	V3-V2-V4-V1	5	V3-V2-V4-V1	0
V3-V4-V1-V2	0	V3-V4-V1-V2	0	V3-V4-V1-V2	0	V3-V4-V1-V2	60	V3-V4-V1-V2	110	V3-V4-V1-V2	0
V3-V4-V2-V1	1	V3-V4-V2-V1	3	V3-V4-V2-V1	0	V3-V4-V2-V1	265	V3-V4-V2-V1	82	V3-V4-V2-V1	0
V4-V1-V2-V3	13	V4-V1-V2-V3	88	V4-V1-V2-V3	0	V4-V1-V2-V3	35	V4-V1-V2-V3	1195	V4-V1-V2-V3	18
V4-V1-V3-V2	4	V4-V1-V3-V2	534	V4-V1-V3-V2	1	V4-V1-V3-V2	14	V4-V1-V3-V2	129	V4-V1-V3-V2	15
V4-V2-V1-V3	2	V4-V2-V1-V3	0	V4-V2-V1-V3	0	V4-V2-V1-V3	12	V4-V2-V1-V3	1607	V4-V2-V1-V3	18
V4-V2-V3-V1	1	V4-V2-V3-V1	276	V4-V2-V3-V1	0	V4-V2-V3-V1	23	V4-V2-V3-V1	359	V4-V2-V3-V1	0
V4-V3-V1-V2	1	V4-V3-V1-V2	0	V4-V3-V1-V2	0	V4-V3-V1-V2	5	V4-V3-V1-V2	1550	V4-V3-V1-V2	1
V4-V3-V2-V1	2	V4-V3-V2-V1	1	V4-V3-V2-V1	0	V4-V3-V2-V1	3	V4-V3-V2-V1	2334	V4-V3-V2-V1	0

Table S13| Occurrence of the rank orders across subjects and 3 gradients

G1				G2				G3			
SC		CB		SC		CB		SC		CB	
rank combination	frequency	rank combination	frequency	rank combination	frequency	rank combination	frequency	rank combination	frequency	rank combination	frequency
V1-V2-V3-V4	14	V1-V2-V3-V4	7	V1-V2-V3-V4	10	V1-V2-V3-V4	18	V1-V2-V3-V4	8	V1-V2-V3-V4	13
V1-V2-V4-V3	5	V1-V2-V4-V3	1	V1-V2-V4-V3	1	V1-V2-V4-V3	10	V1-V2-V4-V3	0	V1-V2-V4-V3	0
V1-V3-V2-V4	0	V1-V3-V2-V4	0	V1-V3-V2-V4	2	V1-V3-V2-V4	2	V1-V3-V2-V4	2	V1-V3-V2-V4	0
V1-V3-V4-V2	2	V1-V3-V4-V2	2	V1-V3-V4-V2	1	V1-V3-V4-V2	4	V1-V3-V4-V2	0	V1-V3-V4-V2	0
V1-V4-V2-V3	0	V1-V4-V2-V3	0	V1-V4-V2-V3	1	V1-V4-V2-V3	0	V1-V4-V2-V3	0	V1-V4-V2-V3	1
V1-V4-V3-V2	3	V1-V4-V3-V2	2	V1-V4-V3-V2	1	V1-V4-V3-V2	1	V1-V4-V3-V2	1	V1-V4-V3-V2	0
V2-V1-V3-V4	7	V2-V1-V3-V4	7	V2-V1-V3-V4	7	V2-V1-V3-V4	0	V2-V1-V3-V4	5	V2-V1-V3-V4	16
V2-V1-V4-V3	1	V2-V1-V4-V3	6	V2-V1-V4-V3	3	V2-V1-V4-V3	1	V2-V1-V4-V3	2	V2-V1-V4-V3	1
V2-V3-V1-V4	0	V2-V3-V1-V4	0	V2-V3-V1-V4	1	V2-V3-V1-V4	0	V2-V3-V1-V4	1	V2-V3-V1-V4	1
V2-V3-V4-V1	0	V2-V3-V4-V1	3	V2-V3-V4-V1	1	V2-V3-V4-V1	1	V2-V3-V4-V1	0	V2-V3-V4-V1	0
V2-V4-V1-V3	0	V2-V4-V1-V3	0	V2-V4-V1-V3	1	V2-V4-V1-V3	0	V2-V4-V1-V3	0	V2-V4-V1-V3	0
V2-V4-V3-V1	1	V2-V4-V3-V1	0	V2-V4-V3-V1	0	V2-V4-V3-V1	0	V2-V4-V3-V1	1	V2-V4-V3-V1	1
V3-V1-V2-V4	2	V3-V1-V2-V4	0	V3-V1-V2-V4	3	V3-V1-V2-V4	0	V3-V1-V2-V4	2	V3-V1-V2-V4	0
V3-V1-V4-V2	1	V3-V1-V4-V2	1	V3-V1-V4-V2	0	V3-V1-V4-V2	0	V3-V1-V4-V2	0	V3-V1-V4-V2	0
V3-V2-V1-V4	0	V3-V2-V1-V4	0	V3-V2-V1-V4	2	V3-V2-V1-V4	0	V3-V2-V1-V4	1	V3-V2-V1-V4	2
V3-V2-V4-V1	0	V3-V2-V4-V1	2	V3-V2-V4-V1	2	V3-V2-V4-V1	1	V3-V2-V4-V1	0	V3-V2-V4-V1	0
V3-V4-V1-V2	0	V3-V4-V1-V2	0	V3-V4-V1-V2	0	V3-V4-V1-V2	0	V3-V4-V1-V2	0	V3-V4-V1-V2	0
V3-V4-V2-V1	0	V3-V4-V2-V1	1	V3-V4-V2-V1	1	V3-V4-V2-V1	1	V3-V4-V2-V1	1	V3-V4-V2-V1	0
V4-V1-V2-V3	0	V4-V1-V2-V3	0	V4-V1-V2-V3	1	V4-V1-V2-V3	1	V4-V1-V2-V3	3	V4-V1-V2-V3	0
V4-V1-V3-V2	1	V4-V1-V3-V2	1	V4-V1-V3-V2	0	V4-V1-V3-V2	1	V4-V1-V3-V2	0	V4-V1-V3-V2	2
V4-V2-V1-V3	0	V4-V2-V1-V3	2	V4-V2-V1-V3	0	V4-V2-V1-V3	0	V4-V2-V1-V3	1	V4-V2-V1-V3	0
V4-V2-V3-V1	1	V4-V2-V3-V1	3	V4-V2-V3-V1	0	V4-V2-V3-V1	0	V4-V2-V3-V1	1	V4-V2-V3-V1	0
V4-V3-V1-V2	1	V4-V3-V1-V2	0	V4-V3-V1-V2	0	V4-V3-V1-V2	0	V4-V3-V1-V2	3	V4-V3-V1-V2	1
V4-V3-V2-V1	5	V4-V3-V2-V1	3	V4-V3-V2-V1	3	V4-V3-V2-V1	3	V4-V3-V2-V1	12	V4-V3-V2-V1	3

Table S14 | Estimated marginal means for minimum distances in G1 as a function of group and ROI.

ROI	group	response	SE	df	lower.CL	upper.CL
V1	CB	0.1102	0.0240	199	0.0718	0.1693
V1	SC	0.3728	0.0783	199	0.2464	0.5640
V2	CB	0.0983	0.0214	199	0.0640	0.1509
V2	SC	0.1422	0.0299	199	0.0940	0.2151
V3	CB	0.0636	0.0138	199	0.0414	0.0976
V3	SC	0.1207	0.0254	199	0.0798	0.1827
V4	CB	0.1232	0.0268	199	0.0802	0.1891
V4	SC	0.1408	0.0296	199	0.0931	0.2131

Table S15 | Results of post hoc tests assessing the effect of group on minimum distances in G1 within each ROI.

ROI	ratio	SE	df	t-ratio	p-value
V1	0.543	0.186	207, 1	-1.778	0.308
V2	0.683	0.235	207, 1	-1.109	0.806
V3	1.369	0.470	207, 1	0.916	0.806
V4	1.447	0.497	207, 1	1.076	0.806

Table S16| Estimated marginal means for minimum distances in G2 as a function of group and ROI.

ROI	group	response	SE	df	lower.CL	upper.CL
V1	CB	0.0702	0.01690	183	0.0437	0.1129
V1	SC	0.1250	0.02904	183	0.0790	0.1976
V2	CB	0.0592	0.01425	183	0.0368	0.0952
V2	SC	0.0624	0.01451	183	0.0395	0.0987
V3	CB	0.0867	0.02088	183	0.0539	0.1395
V3	SC	0.0377	0.00875	183	0.0238	0.0596
V4	CB	0.1445	0.03478	183	0.0899	0.2323
V4	SC	0.0578	0.01344	183	0.0366	0.0915

Table S17 | Results of post hoc tests assessing the effect of group on minimum distances in G2 within each ROI.

ROI	ratio	SE	df	t-ratio	p-value
V1	**0.296**	**0.089**	**199, 1**	**-4.029**	**< 0.001**
V2	0.691	0.209	199, 1	-1.221	0.447
V3	0.527	0.159	199, 1	-2.121	0.106
V4	0.875	0.264	199, 1	-0.443	0.658

Table S18 | Estimated marginal means for minimum distances in G3 as a function of group and ROI.

group	ROI	response	SE	df	lower.CL	upper.CL
CB	V1	0.070	0.017	183.136	0.044	0.113
SC	V1	0.125	0.029	183.136	0.079	0.198
CB	V2	0.059	0.014	183.136	0.037	0.095
SC	V2	0.062	0.015	183.136	0.039	0.099
CB	V3	0.087	0.021	183.136	0.054	0.139
SC	V3	0.038	0.009	183.136	0.024	0.060
CB	V4	0.144	0.035	183.136	0.090	0.232
SC	V4	0.058	0.013	183.136	0.037	0.091

Table S19 | Results of post hoc tests assessing the effect of group on minimum distances in G3 within each ROI.

ROI	ratio	SE	df	t-ratio	p-value
V1	0.562	0.188	183, 1	-1.723	0.173
V2	0.949	0.317	183, 1	-0.158	0.875
V3	**2.302**	**0.77**	**183, 1**	**2.492**	**0.041**
V4	**2.499**	**0.836**	**183, 1**	**2.737**	**0.027**

Table S20 | Anova and Tukey-Kramer post-hoc tests of the mean absolute coupling values across groups and gradients.

	Sum Sq.	df	Mean Sq.	F	p-value
Group	0.03	1	0.03	2.81	0.090
Gradient	7.54	2	3.77	276.01	< 0.001
Group X Gradient	3.45	2	1.72	63.62	< 0.001
Error	29.42	2154	0.01		
Total	40.46	2159			

Table S21 | Estimated value of difference (EVD) across gradients and groups.

comparison	lower CL	estimate	upper CL	p-value
SC-G1 X CB-G1	0.0924	0.1172	0.1421	< 0.001
SC-G1 X SC-G2	0.1855	0.2103	0.2352	< 0.001
SC-G1 X CB-G2	0.1126	0.1374	0.1622	< 0.001
SC-G1 X SC-G3	0.1767	0.2016	0.2264	< 0.001

SC-G1 X CB-G3	0.1578	0.1826	0.2074	< 0.001
CB-G1 X SC-G2	0.0683	0.0931	0.1179	< 0.001
CB-G1 X CB-G2	-0.0047	0.0202	0.045	0.1886
CB-G1 X SC-G3	0.0595	0.0843	0.1092	< 0.001
CB-G1 X CB-G3	0.0405	0.0653	0.0902	< 0.001
SC-G2 X CB-G2	-0.0978	-0.0729	-0.0481	< 0.001
SC-G2 X SC-G3	-0.0336	-0.0088	0.0161	0.9164
SC-G2 X CB-G3	-0.0526	-0.0277	-0.0029	0.0181
CB-G2 X SC-G3	0.0394	0.0642	0.089	< 0.001
CB-G2 X CB-G3	0.0204	0.0452	0.07	< 0.001
SC-G3 X CB-G3	-0.0438	-0.019	0.0058	0.2471

Table S22 | Regions that showed significant differences in structure-function coupling.

region	hemi	yeo	SC	CB	Difference	p (uncorr)	p (corr)
V2	L	VIS	-0.475	0.328	-0.803	0.001	0.043
V3	L	VIS	-0.505	0.236	-0.741	0.002	0.044
IPS1	L	DAN	-0.405	0.398	-0.803	0.001	0.043
FFC	L	VIS	-0.42	0.315	-0.734	0.003	0.045
STV	L	DMN	0.428	-0.333	0.761	0.002	0.044
8BL	L	DMN	0.438	-0.31	0.748	0.002	0.044
47s	L	DMN	0.476	-0.542	1.019	0	0.004
Pir	L	LIN	0.184	-0.514	0.699	0.003	0.047
STSvp	L	DMN	0.17	-0.675	0.845	0	0.014
VMV1	L	VIS	-0.488	0.244	-0.732	0.002	0.044
VMV3	L	VIS	-0.469	0.278	-0.747	0.002	0.044
V3CD	L	VIS	-0.436	0.329	-0.765	0.002	0.044
VVC	L	VIS	-0.498	0.345	-0.843	0	0.031
STSva	L	DMN	0.095	-0.582	0.677	0.003	0.046
V2	R	VIS	-0.58	0.41	-0.99	0	0.004
V3	R	VIS	-0.558	0.216	-0.774	0.001	0.043
V4	R	VIS	-0.521	0.183	-0.704	0.003	0.046
IPS1	R	DAN	-0.437	0.352	-0.789	0.001	0.044
FFC	R	VIS	-0.56	0.145	-0.705	0.003	0.044
V3B	R	VIS	-0.511	0.328	-0.839	0	0.031
PIT	R	VIS	-0.478	0.294	-0.771	0.001	0.044
ProS	R	VIS	-0.088	0.603	-0.691	0.002	0.044
V3CD	R	VIS	-0.452	0.312	-0.764	0.002	0.044

VVC	R	VIS	-0.522	0.235	-0.757	0.001	0.044
STSva	R	DMN	0.302	-0.426	0.728	0.003	0.046